Experimental Characterization and Modeling of Galfenol (FeGa) Alloys for Sensing

A Thesis

Presented in Partial Fulfillment of the Requirements for the Degree Master of Science in the Graduate School of The Ohio State University

By

Travis W. Walker, B.S.

Graduate Program in Mechanical Engineering

The Ohio State University

2012

Master's Examination Committee:

Dr. Marcelo J. Dapino, Advisor

Dr. Xiaodong Sun

Abstract

Magnetostrictive materials are a class of smart materials that have the capability to convert mechanical energy to magnetic energy and vice versa. This transfer of energy makes these materials good candidates for both sensing and actuation applications. A device constructed of one of these materials could perform the same function as current parts that utilize several components which would increase the durability, and lead to smaller components. The potential uses of these materials cover a broad range of applications, including self-sensing actuators due to the fact that smart materials are bidirectionally-coupled. An additional benefit in relation to sensors is that magnetostrictive materials can operate in a non-contact fashion. Measuring the magnetic response to a stress input can be done using different non-contact techniques which would reduce the complexity from current force sensors. Galfenol, an alloy of iron and gallium, is a promising material for both actuation and sensing due to the moderately large strain it exhibits under a magnetic field combined with the material's mechanical robustness. Galfenol has properties similar to steel which allow for machining, extruding, and other load bearing applications. These mechanical properties make Galfenol unique relative to other smart materials, which generally are brittle.

This research looks to further the study of Galfenol by documenting the behavior of $Fe_{81.6}Ga_{18.4}$ under various loading conditions in relation to the development of a force

sensor. The characterization of these alloys involves applying a stress to the sample and measuring the corresponding change in magnetization. Both major and minor loop responses were observed over a range of stresses and fields. These were compared for sensitivity and used to determine model parameters. Additional minor loop testing was conducted at high frequencies to determine the material's dynamic behavior as a sensor. The sensitivity was observed to decrease with increasing frequency. Using a modulation technique allowed for a means of relating the input stress to the output voltage while being independent of frequency when that frequency was in a range well below the frequency of the carrier frequency. The relationship between the input stress and output magnetization was also compared with constitutive models for Galfenol to further validate the models to be used towards the development of a force sensor. The relationship between the input stress and the output magnetization is non-linear and exhibits hysteresis, so the characterization of these responses will be beneficial in the creation of sensors utilizing Galfenol.

Acknowledgments

This research would not have been possible without the help of many intelligent and encouraging people. I would first like to thank my advisor, Dr. Marcelo Dapino, for his support and advice thoughout the course of this research. His guidance and insight were immensely helpful to this project. I would also like to thank him for providing me the opportunity to be involved in this project. In addition, I thank the Department of Mechanical and Aerospace Engineering at The Ohio State University. Both the department and the university were great resources with equipment and personnel. My undergraduate career at The Ohio State University provided a solid background for tackling this research project. My colleagues in the Smart Material and Structures Laboratory have also been most helpful through this process. I would especially like to thank Dr. Ling Weng and Zhangxian Deng for their help. They were instrumental in many aspects of this project and provided a great sounding board for ideas.

In addition to the people that I worked with at The Ohio State University, I would also like to thank my family and friends. My friends have provided support in the form of fun activities to recharge the batteries. My fiancée, Stephanie, has been encouraging throughout the process. Even if she didn't understand what I was doing, she was always willing to listen and provide words of encouragement. My family has been a constant source of encouragement in everything that I've done. My

parents have been one of the biggest influences in my life by continually pushing me to succeed. The hard work and dedication that is exhibited in their lives is something that I strive for everyday. I greatly appreciate all that they have done for me this far in my life, and it is because of their hard work that I was able to attend college and study engineering at The Ohio State University. I would once again like to take this opportunity to thank everyone in my life for helping me get to the place I am today.

Vita

July 18,1988	Born - Findlay, OH
June 2007	Liberty-Benton High School, Valedictorian
June 2011	B.S. Mechanical Engineering, Summa Cum Laude, The Ohio State University
2011 - Present	Graduate Research Associate, The Ohio State University

Fields of Study

Major Field: Mechanical Engineering

Studies in Smart Materials and Structures: Dr. Marcelo Dapino

Table of Contents

Page

List of Tables

List of Figures

Chapter 1: INTRODUCTION

1.1 Background

Two widely used aspects of engineering are sensing and actuation. Methods of sensing are help determine the forces and loads acting on different components. Actuation helps to create moving mechanisms in engineered structures, and can be used to control the function of the device in which they are implemented. As research in actuation and sensing solutions using common materials has progressed, several limitations have been discovered. These shortcoming have prompted an interest in smart materials. The main characteristic of smart materials is the interaction between two different states. For example, some smart materials have a distinct relationship between electrical and mechanical regimes whereas others exhibit a relationship between magnetic and mechanical regimes. Research into the potential of smart materials has shown increasing promise in the aerospace, automotive, and medical fields.

Smart materials exhibit a controlled change in some property in response to an external stimulus. This can be either temperature, electric, or magnetic. Understanding this change can lead to better design and application of smart materials for different problems. Two of the main smart materials currently being used in applications are shape memory alloys (SMAs) and piezoelectric materials. SMAs respond to a change

in temperature, and are best suited for low frequency, high strain applications. Piezoelectric materials respond to a change in electric field, and are best suited for high frequency, low strain applications [2].

Magnetostrictive materials deform in the presence of a magnetic field, and change their magnetization with the application of stress. The magnetic field induced deformation, or strain, is called magnetostriction, and gives these materials their name. The combination of actuation and sensing could be used in conjunction to create more compact and durable components because one device could serve multiple purposes. The actuation characteristics have potential uses in vibration control, sonar transducers, and much more. The sensing characteristics could be valuable in such things as non-contact force or torque sensors as well as acoustic sensors [6].

Magnetostriction was first discovered in the 1840's by James P. Joule. He discovered magnetostriction in common materials such as nickel and iron. The strain was on the order of 10×10^{-6} and found uses in telephone receivers and hydrophones. [10] In the 1970's, "giant" magnetostrictive materials were synthesized by adding rare earth elements such as terbium (Tb) and dysprosium (Dy) to iron. The proper ratio of these elements to iron was determined and the Naval Ordnance Laboratory developed Terfenol-D (terbium: Ter; iron: Fe; Naval Ordnance Laboratory: NOL; dysprosium: D) which exhibits a magnetostriction of 1600×10^{-6} under a saturation magnetic field of 160 kA/m. This material has been commercially available since the 1980's [9]. The large magnetostriction makes this material a good potential candidate for sensing and actuation; however this material is also very brittle which limits its use in many applications.

Galfenol alloys ($Fe_{1-x}Ga_x$) where the gallium content, x, varies between 12 and 20% were also developed through scientific research by the Naval Ordnance Laboratory. These alloys have mechanical properties that are far superior to those in Terfenol-D. Galfenol has a mechanical robustness similar to steel while exhibiting a moderate magnetostriction at low saturation fields. The magnetostriction for Galfenol is around 300×10^{-6}. The unique properties of Galfenol makes it a potential candidate for shock-tolerant adaptive structures, as well as sonar transducers with load bearing capability [15]. Galfenol is a promising alloy that still needs to be better understood for use in real world applications.

1.2 Literature Review

1.2.1 Magnetostrictive Principles

Magnetostrictive materials show a coupling between the mechanical and magnetic regimes. Making use of the actuation effect (inverse effect) means that a field is applied and the magnetic domains align themselves with the direction of the magnetic field in the material. This alignment of domains causes a change in the overall dimensions of the material, and thus causes a strain. The sensing effect (direct effect) uses the fact that as a stress is applied to a magnetized sample, the magnetic moments that are aligned with the magnetic field are forced to rotate with the stress. For a compressive loading this means that the moments rotate from the aligned state to a state where they are perpendicular with the applied field. In these materials, the magnetization ($\mathbf{M}$), or $\mathbf{B} = \mu_0(\mathbf{H} + \mathbf{M})$, and strain ($\mathbf{S}$) respond to a changes in magnetic field ($\mathbf{H}$) and stress ($\mathbf{T}$) in a non-linear manner that depends on the

history of the material. The nonlinearities are caused by anisotropy, and saturation. Magnetostrictive materials are also directionally dependent [2, 14].

In dealing with the direct effect of magnetostrictive materials a magnetic field is first applied to the material. This field can be measured in a variety of different ways; however one means of visualizing a magnetic field is through the use of iron filings, which align themselves with the direction of the magnetic field. A magnetic field is a vector caused by an electric charge in motion and is dependent on the size and distribution of currents in a material. Magnetic flux is the amount of magnetic field flowing through a surfaces and is dependent on the properties of the material [18].

The magnetic domains are composed of magnetic moments which are aligned parallel to each other within a domain; under no applied stress, domains are oriented such that zero net magnetization is present. The process of magnetizing a material is therefore the reorientation of domains. The magnetic anisotropy in materials leads to certain easy axis that is dependent on the crystal structure of the material. In this manner it is difficult to magnetize a material along one of the hard axes because of the anisotropy energy that must be overcome. The actual process of magnetization utilizes two different mechanisms.

The first is domain wall motion and is associated with the growth of domains that are in the direction of the applied field at the expense of other domains. This occurs generally at small fields. Domain rotation requires more energy and creates a more gradual change in the magnetization with an increasing field. In Galfenol, these mechanisms have been found to also be dependent on the alloy being used.

Evans [14] showed that Galfenol with 18.4 at. % gallium has a higher anisotropy energy which limits the domain rotation, and thus forces the magnetization process

to utilize the domain wall motion. Galfenol with 20.9 at % gallium on the other hand has a lower anisotropy and the magnetization process involves a considerable amount of domain rotation. Sensing the difference in mechanisms relates to the difference in sensitivity of the material to stress. The lower percentage gallium alloy is more sensitive to stress as compared to the higher quantity gallium alloy, but has a limited range of linear response [21, 14].

1.2.2 Quasi-Static Characterization

Past research has focused on the characterization and material properties of Galfenol. One area of importance is the maximum value of magnetostriction based on the amount of gallium present in the alloy. It has been observed that the maximum value occurs between 17 at.% and 19 at.% depending on the processing technique used [12]. For this reason, much of the subsequent research makes use of alloys near these values. The results of this study can be seen in Figure 1.1.

Kellogg et al. tested both single crystal and polycrystalline samples of $Fe_{81}Ga_{19}$ and observed that Galfenol is temperature insensitive. Over a range of -21°C to 80°C, there was a small 12% variation in magnetostriction and a 3.6% variation in the saturation magnetization. This study also showed that the field required for saturation increased with an increase in the compressive loading of the sample and that the hysteretic losses in Galfenol where significantly smaller than those in Terfenol-D. They also found that the magnetostriction in polycrystalline samples was higher than in single crystals whereas the magnetization was lower [20].

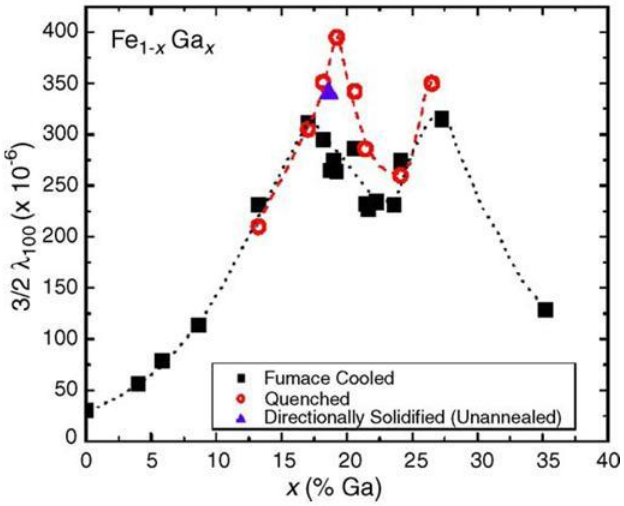

Figure 1.1: Magnetostriction for Different Compositions of % at. Ga [12]

Another area of interest with Galfenol has been to characterize the material properties. In this work, the material is subjected to a varying field under different constant stress loads to obtain a relationship between the magnetization in the sample with the field applied as a function of the stress in the sample. The magnetostriction is also measured during these tests, and the two relationships (Magnetization vs. Field, and Strain vs. Field) make up the actuation measurements of a material. For sensing, the varying input is stress while the sample held at a constant field. The Magnetization vs. Stress and Strain vs. Stress curves provide the characteristic curves for this characterization. Evans et al [14], and Mahadevan et al. [21] have looked at these curves for various types of Galfenol alloys.

1.2.3 Galfenol Modeling

The next step in the understanding of Galfenol alloys is creating a comprehensive model to represent the relationship between the magnetic and mechanical regimes. Atulasimha et al. [4] have modeled both the actuation and sensing in polycrystalline samples of Galfenol using an energy-weighted average modeling technique. This uses a Boltzmann distribution for the weighting functions and includes terms for anisotropy, magneto-mechanical coupling, and magnetic work. The choice of weighting functions was based on the Armstrong model [1]. This initial work was an anhysteretic for Galfenol. Atulasimha et al. [3] combined this modeling with a hysteresis model to describe the actuation process. The main drawback of these modeling techniques was the efficiency and speed of implementation.

Evans et al. has developed a constitutive model that can accurately represent hysteresis, stress and annealing induced anisotropies, and thermal relaxation effects. This model greatly improves the efficiency while maintaining a high level of accuracy. The modeling used in this thesis makes use of the non-linear Discrete Energy Average Method. In this modeling, the energy in a domain is defined locally and then minimized about the easy axes of rotation. This method was developed to be more efficient in modeling the complex relationship between the mechanical and magnetic regimes. This is due to the fact that the energy is defined locally about the known preferred orientations. This model is based on a formal thermodynamic construction to deal with hysteresis and anisotropy [14].

1.3 Objectives and Thesis Organization

The first objective of this research is to characterize the behavior of the material for sensing. For this research, a sample of $Fe_{81.6}Ga_{18.4}$ highly textured polycrystalline <100> oriented research grade sample was characterized. This characterization focused on the sensing characteristics of the material, and thus, the magnetization vs. stress curves were the relationship of interest. The characterization involved looking at both major and minor loop behavior of the material. The sensitivity to stress was also observed to create a better understanding for potential use in force sensing devices. The characterization was performed in both compression and tension to understand the full range of operation conditions Galfenol might experience. The results of this characterization objective are discussed in further detail in Chapter 2.

The second objective is to expand the characterization into the realm of dynamic operation. This involved looking at how the response varied with respect to the frequency of the input stress signal. The first test looked at relatively low frequencies and how to manage the change in response. To further expand this study, the frequency range was increased and the results observed in terms of both sensitivity and hysteresis loss. Another aspect of this objective included the use of a modulation technique as described by Evans et al. [14]. Chapter 3 discusses the testing involved in the dynamic characterization.

The third objective of this thesis is to look at the power requirements for the transducer being used. For Galfenol to be a realistic replacement for a typical force sensor, it must be efficient. This means that the power requirements to operate the sensor must be minimized. Chapter 4 discusses the current power requirements

for a force sensor making use of the stress-dependent susceptibility technique. This technique makes use of modulation as described in Chapter 3.

The final objective is to implement the characterization data into existing models for Galfenol. The transducer used in the characterization was modeled in COMSOL, and using MATLAB user-defined functions created by Chakrabarti et al. [7], the transducer was simulated. The MATLAB functions make use of the model created by Evans which are then integrated into the COMSOL framework. Modeling transducers in COMSOL would help in the design process and help to reduce cost. This process is outlined in Chapter 5.

Chapter 2: MAJOR AND MINOR LOOPS

2.1 Overview

In terms of magnetostrictive materials, the main quantities that are of interest are the magnetization and strain as a function of both stress and applied magnetic field. One of the inputs is often held constant while the other is varied, and the resulting changes in the output variables are measured. For actuation measurements, the field is varied while the stress is held constant. The opposite is true of sensing curves. In this research the focus is on the sensing characteristics of the material. In the following section, both the major and minor loops of the material are reported for different bias fields.

One issue to consider when characterizing sensing curves is how the field is generated. With a constant current applied to the excitation coils, the field in the sample changes with the applied stress. This is due to the change in reluctance of the transducer circuit. For this reason, measurements taken with constant current applied to the drive coils of the circuit also are affected by the circuit itself. In many cases it is necessary to investigate how the material itself responds. To accomplish this experimentally, a feedback controller is implemented to create a constant field in the

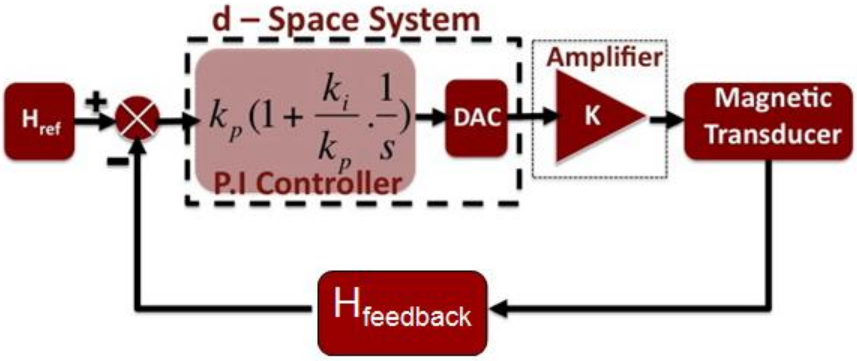

Figure 2.1: PI Controller Used to Keep Constant Magnetic Field; (kp = 0.35 and ki = 0.55) [21]

sample as the stress is applied. This controller was designed by Mahadevan et al. [21]. A block diagram of this controller is seen in Figure 2.1.

2.2 Major Loops

The major loops are associated with a wide range of input stresses. These curves give the material properties of the specific alloy and these properties can be used in the modeling of transducers that make use of this material. The major loops described below show the magnetization versus stress curves for different bias fields. The bias fields range from 0.80 kA/m (10 Oe) to 8.0 kA/m (100 Oe), and the stress goes from approx 65 MPa to -65 MPa. An explanation of the experimental set-up and procedure is detailed below.

2.2.1 Test Set-up

For this test, the Galfenol sample was placed inside the transducer as shown in Figure 2.2. This transducer was then placed between two plates made of aluminum.

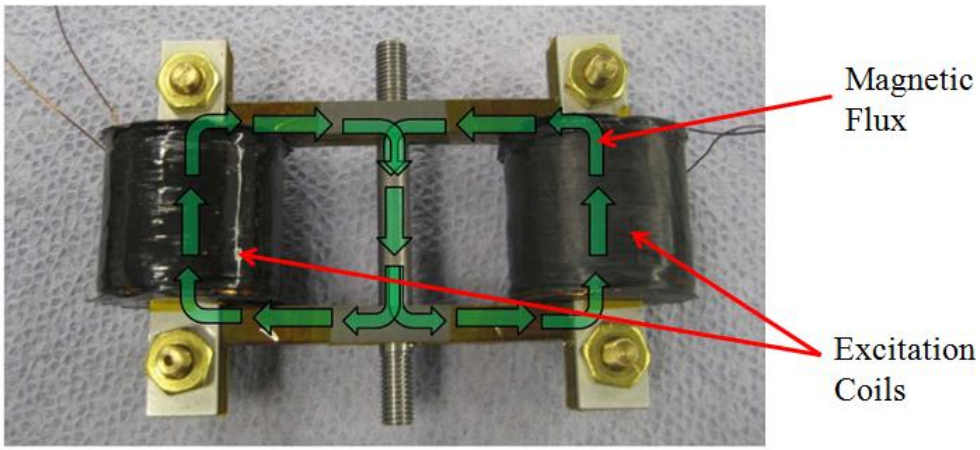

Figure 2.2: Transducer for Material Characterization with Flux Return Path

The aluminum plates are non-magnetic, and thus, force the flux created by the drive coils to follow the steel flux circuit into the center of the sample. The aluminum plates were both affixed to the load frame by clamping them to another aluminum plate attached to the standard rods of the load frame. Figure 2.3 shows the transducer with the two aluminum circular plates attached. Two larger aluminum plates with stand-offs were attached to the rods of the load frame, and the circular plates were positioned between the stand-offs so that a connector could be bolted to them, and thus, clamp the circular plates to the rectangular ones. In this manner, both tensile and compressive loads could be applied to the sample. The sample was first placed in a state of zero load and at remanence. From this point, the sample was again saturated, and the current reduced until the desired field was achieved at zero stress.

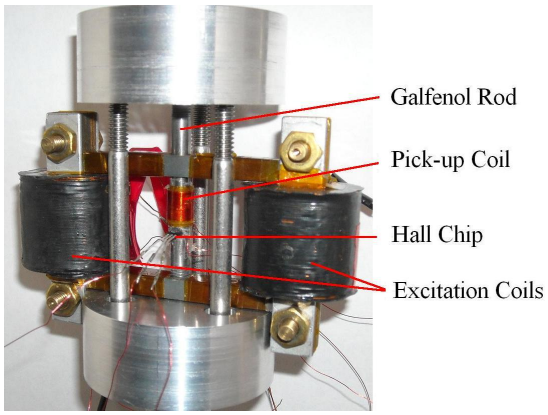

Figure 2.3: Experimental Set-up For Characterization

For the characterization curves the load was applied using the Test Resources R Series Controller. The load was applied sinusoidally with a frequency of 0.05 Hz and an amplitude of approximately 65 MPa. Throughout this loading, the value of magnetic flux density, magnetic field, and load were recorded. Flux density was recorded using a Walker Scientific 5D integrating flux meter and a pick-up coil wrapped around the center of the sample. The field was measured using an Allegro A1322LUA-T hall chip. The force was measured by the built in load cell of the load frame. The load frame was operated in load control so that each major loop would have the same stresses for equal comparison. The constant field testing was conducted in a similar manner, except that rather than keep the current to the excitation coils constant, the PI controller (Figure 2.1), implemented through dSpace, was used to adjust the current to keep the field constant. The same stress input was used, and the flux density, field, and load were recorded. After testing was complete, the magnetization of the sample were found by subtracting the field from the flux density. The results were then plotted and can be found in the following section.

2.2.2 Major Loop Results

The major loop curves of Magnetization vs. Stress are shown in Figure 2.4 and Figure 2.5 for both constant current to the drive coils as well as constant field in the sample. These curves show that the slope of the linear region is steeper for the constant field measurements. This difference is due to the changing reluctance of the system due to the changing permeability of Galfenol in the constant current testing. In this set-up, the stress on the sample causes a changing reluctance in the Galfenol sample, and the field in the sample thus increases. The field measurements for the constant current test can be seen in Figure 2.6. The change in field leads to a smaller change in the overall magnetization as the compressive stress is applied. For the constant current tests, the current values were chosen to create a specific initial bias field at zero stress. The same fields were used in the constant field tests. The fields were chosen to range from 10 Oe to 100 Oe in increments of 10 Oe. This corresponds to 0.8 kA/m, 1.6 kA/m, 2.4 kA/m, 3.2 kA/m, 4.0 kA/m, 4.8 kA/m, 5.6 kA/m, 6.4 kA/m, 7.2 kA/m, and 8.0 kA/m in SI units. These units will be used in all further figures. For the constant current tests, the currents were found to be 98 mA, 204 mA, 288 mA, 338 mA, 0.384 mA, 426 mA, 464 mA, 508 mA, 550 mA, and 596 mA.

Other noticeable characteristics of the major loops are the location of the burst region as well as the value stress-induced saturation. The field-induced saturation (at low compressive stresses and tensile stress) is very similar for all cases except those for low bias fields. This is because the field is not strong enough to cause saturation and the tensile stresses do not aid as much in the magnetization process. The field-induced saturation for the higher bias fields corresponds to the case where all of the magnetic moments are aligned in the direction of the field.

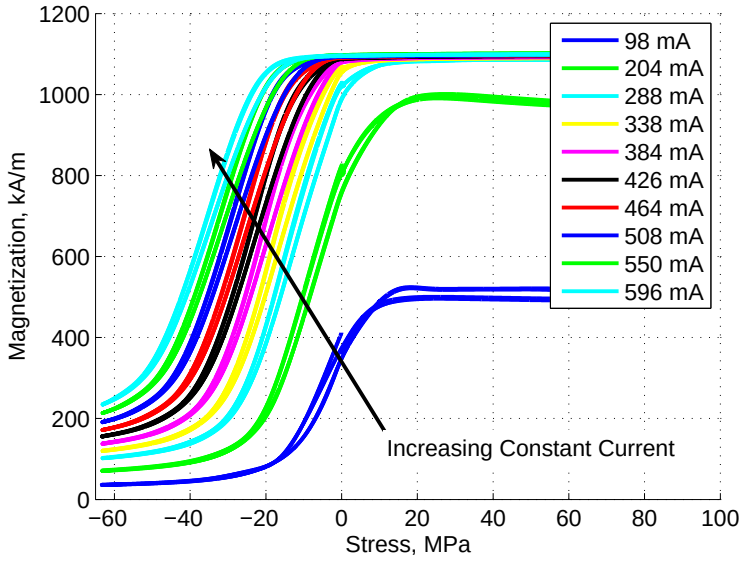

Figure 2.4: Magnetization vs. Stress for Constant Current Excitation (98, 204, 288, 338, 384, 426, 464, 508, 550, 596 mA) - Initial Bias fields (0.8, 1.6, 2.4, 3.2, 4.0, 4.8, 5.6, 6.4, 7.2, 8.0 kA/m)

The stress-induced saturation (at high compressive stresses) is slightly different for each bias field. The stress-induced saturation is caused because the compressive stress has aligned all of the magnetic moments perpendicular to the field direction. The difference in fields is due to the fact that the bias field produces a small magnetization even at high stresses. Moreover, this value is slightly higher for higher bias fields because the strength of the magnetic energy is working against the stress input.

The other interesting characteristic of the major loops is the location of the burst region. The burst region is where the stress is large enough to begin altering the magnetization of the material. At this location the magnetic field energy and anisotropy energy are not sufficient enough to oppose the mechanical input. From these curves it can be observed that the burst region moves to the left with higher bias fields.

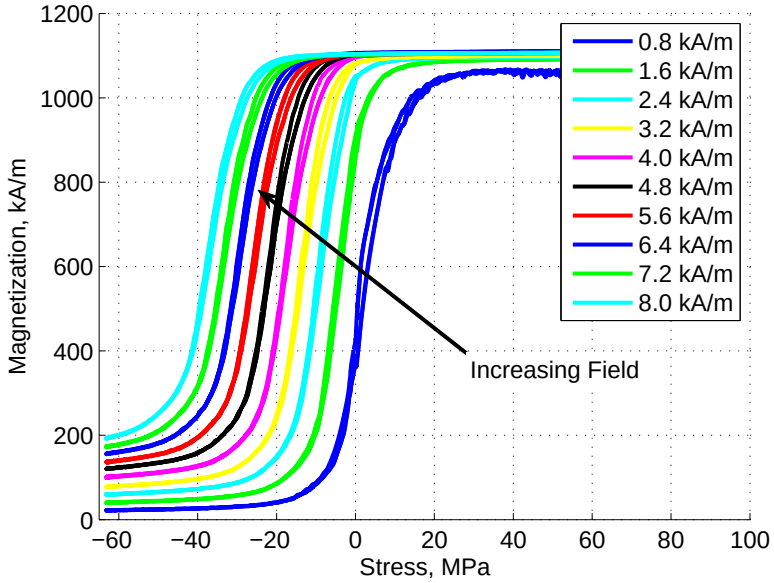

Figure 2.5: Magnetization vs. Stress for Constant Field Excitation - Fields (0.8, 1.6, 2.4, 3.2, 4.0, 4.8, 5.6, 6.4, 7.2, 8.0 kA/m)

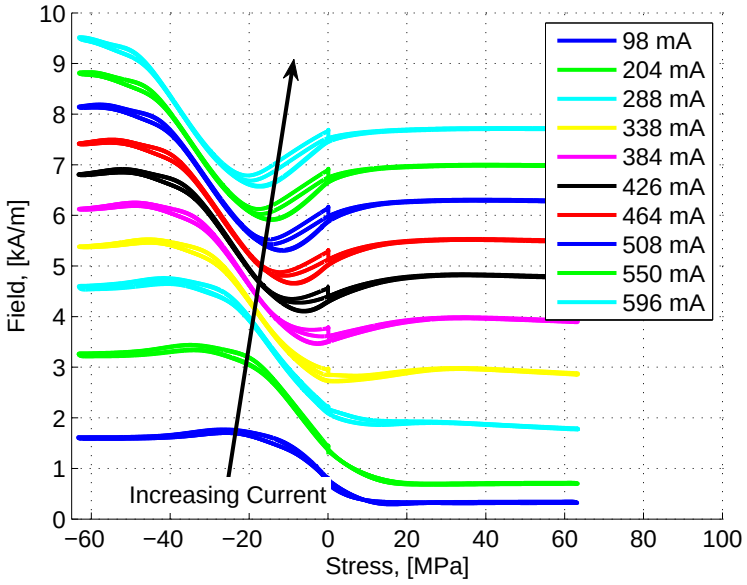

Figure 2.6: Field vs. Stress for Constant Current Excitation

2.2.3 Sensitivity

The slope of the Magnetization vs. Stress curves is the sensitivity of the material and is plotted in terms of flux density in Figure 2.7 and Figure 2.8 for the constant current and constant field tests respectively. These plots were made with the average sensitivity between when the stress was increasing and decreasing. The difference between the increasing and decreasing stress can be seen in Figure 2.9 along with the comparison between constant field and constant current. Three fields were chosen for clarity purposes.

It is clear that the constant field tests have a higher sensitivity than the constant current tests. Also, there are two sets of lines for each field. These correspond to the sensitivity difference depending on the direction of stress input. The solid lines indicate the sensitivity when the stress is becoming more compressive while the dashed lines represent the return path when the compressive stress is being removed.

These figures show that the the maximum value of sensitivity is higher for the constant field measurements, and the stress value associated with that point is moved closer to the right. These figures also show that the peak sensitivity decreases with the increasing bias field. The peak sensitivity corresponds to the beginning of the burst region when the compressive stress balances the magnetic and anisotropy energy in the sample. The difference between the dashed and solid lines is caused by the hysteresis in the flux density measurements. This hysteresis is caused by the hysteretic and nonlinear behavior of Galfenol.

The sensitivity was calculated numerically from the change in the flux density with respect to the change in stress. Large errors can be introduced using this method due to noise in the data signals. To combat this error, a moving average was implemented

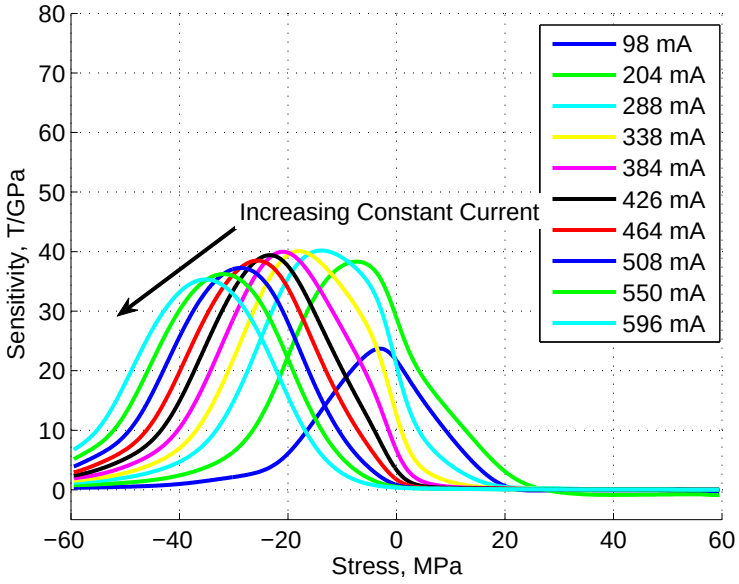

Figure 2.7: Sensitivity vs. Stress for Constant Current Excitation

in MATLAB. The total data set consisted of two cycles of stress input and 92,000 data points. To smooth the data, a window of 500 points was used for the moving average. This smoothed out the data and allowed for more accurate calculation of the sensitivity.

2.2.4 Comparison with Actuation

To validate the testing procedure, the sensing and actuation curves were compared. The actuation testing was done using the same Test Resources Load Frame with R Series Controller. For these tests, a sinusoidal current was applied to the excitation coils to generate magnetostriction in the sample. The input had a frequency of 0.05 Hz and an amplitude of approximately 1.7 A. This was sufficient to saturate the sample

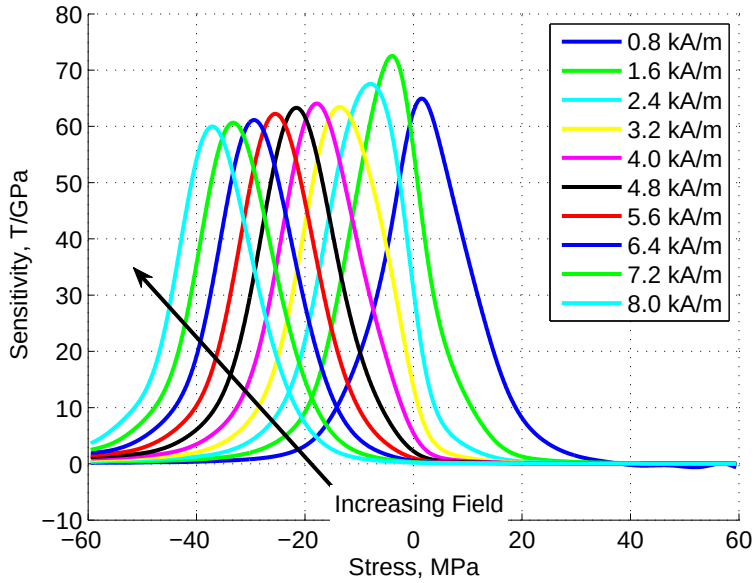

Figure 2.8: Sensitivity vs. Stress for Constant Field Excitation

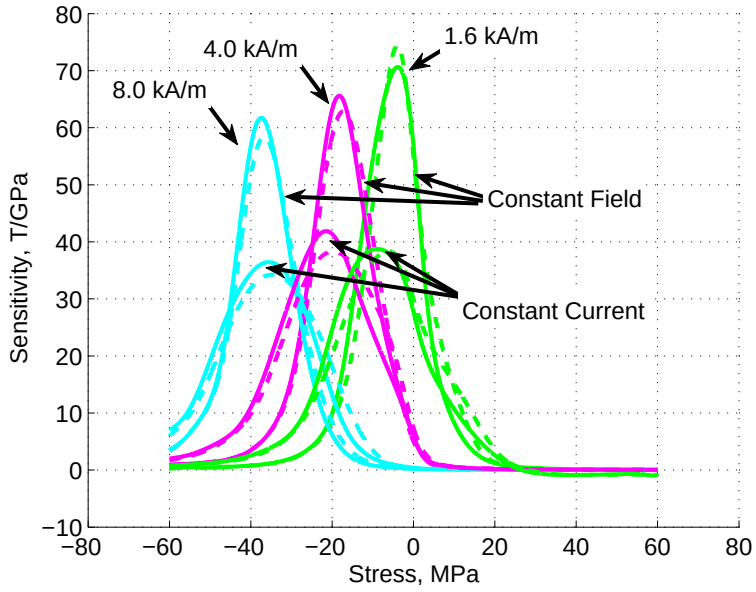

Figure 2.9: Sensitivity vs. Stress Comparison - Dashed: Decreasing Compressive Stress; Solid: Increasing Compressive Stress

at 60 MPa so that a good comparison with the sensing curves could be achieved. The sample was first loaded, placed in a state of remanence, and then loaded to the bias stress. The R Series Controller then held the load constant while the current excitation was applied to the sample.

During the testing, both the flux density and the magnetic field were measured and the magnetization calculated as described above. The load was also recorded to compare with the sensing data. The comparison was done using the anhysteretic curves from both the actuation and sensing data and was found by taking the average between the upper and lower curves. Using an averaging procedure produces some error from the true anhysteretic behavior; however this difference is small. Comparing the two sets of data allows for a direct comparison between the two types of tests to validate the procedure of the sensing curves.

For this comparison, the different stresses from the actuation tests became the common point. The sensing data was then analyzed to find the corresponding field and magnetization at the same stress. These data points were plotted on top of the actuation curves, and are shown in Figure 2.10 and Figure 2.11 for the constant current and constant field tests respectively. There is only one set of actuation data, and the agreement between the actuation and both sensing data helps to validate the testing procedure for the sensing data. The actuation data was collected at different stresses from -60 MPa to 60 MPa in intervals of 10 MPa.

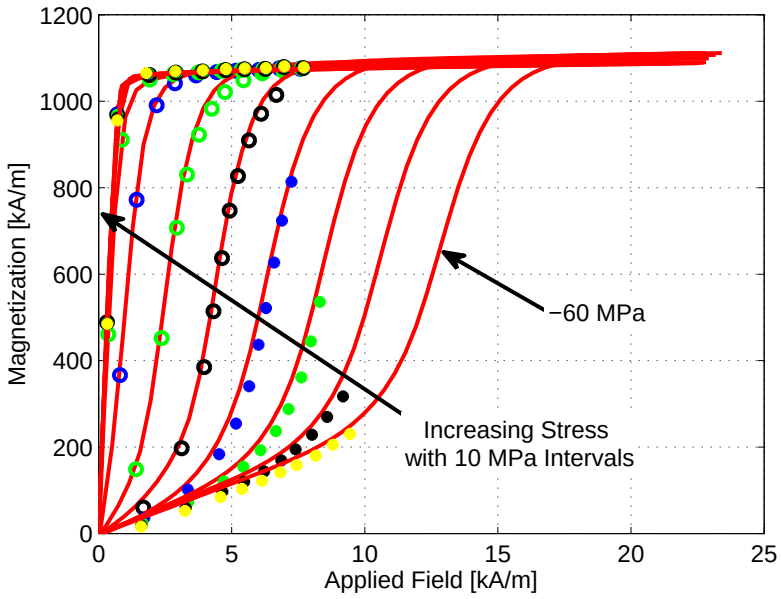

Figure 2.10: Magnetization Comparison Between Actuation and Sensing Testing Procedures with Constant Current Excitation - Lines: Anhysteretic Results of Actuation Testing; Dots: Points Extracted from Sensing Data

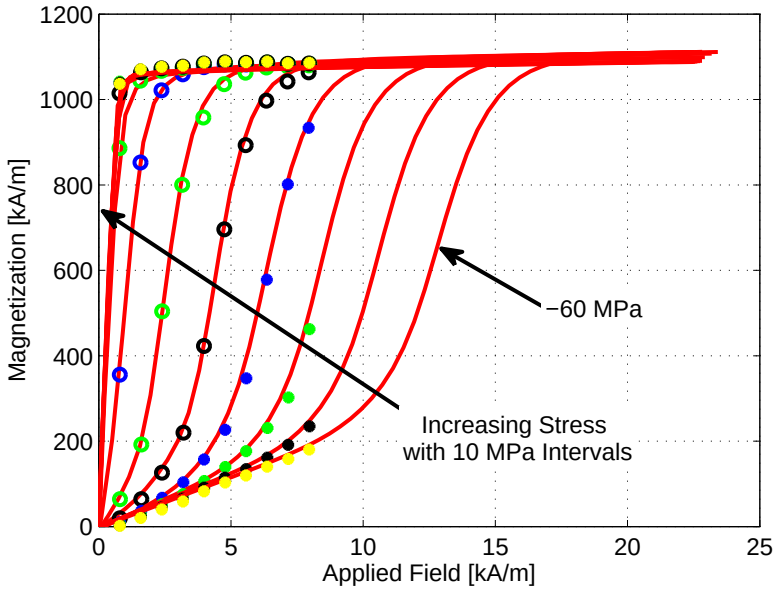

Figure 2.11: Magnetization Comparison Between Actuation and Sensing Testing Procedures with Constant Field Excitation - Lines: Anhysteretic Results of Actuation Testing; Dots: Points Extracted from Sensing Data

2.3 Minor Loops

Minor loops are help in the understanding of the material because in practical applications, these materials will often be operated about a bias point with a small range of operation. This is due to the nonlinear response of the material. Working in the linear region of response allows for quick and accurate implementation. For this reason, the minor loops for this sample of Galfenol were also observed. This allows for a comparison between the major and minor loop data to see how the response differs. It will be also helpful to validate the model with respect to hysteresis.

2.3.1 Test Set-up

The minor loops were conducted in a similar manner to the major loops, with a couple of additional steps, and a narrow range of applied stresses. After reaching remanence, the sample was placed in the machine as described above, a current was applied to saturate the sample, and then returned to the working current as described in the major loop testing. The sample was then subjected to a 1.05 MPa/s ramp loading to the desired stress. From this point a 4 Hz sine wave of amplitude 2.86 MPa was applied for two cycles. The results were calculated in a similar manner to that described above and can be found in the following section. For this testing, six different bias forces were chosen ranging from -40 lbf to -290 lbf in increments of 50 lbf. This corresponds to stresses of -5.6 MPa to -40.6 MPa in increments of 7.0 MPa. The minor loops were chosen in the compressive region because that is where the burst region is located for the different bias fields. With a small stress range, there would be little change in the magnetization in the regions of saturation.

2.3.2 Minor Loop Results

The minor loops for constant field and constant current are plotted below in Figure 2.12 and Figure 2.13 for both constant current and constant field tests. In these figures, the different colors represent different bias stresses. Due to the control of the field, the minor loops for the constant field have very little hysteresis when compared to the constant current measurements. A similar observation can be made for the major loops shown above. Figure 2.12 and Figure 2.13 show the minor loops with out the major loops for clarity purpose. It can also be observed that the minor loops follow a similar trajectory to the major loops seen in the previous section. The

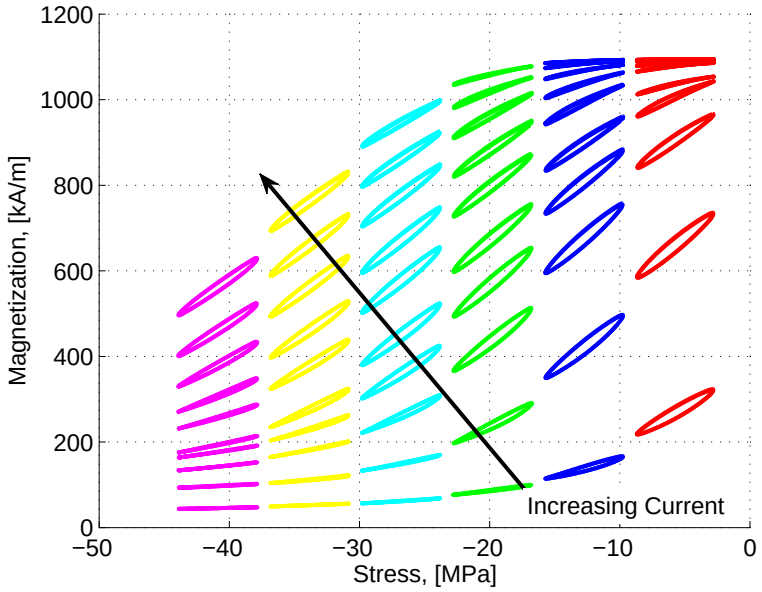

Figure 2.12: Magnetization vs. Stress for Minor Loops with Constant Current Excitation - Bias Stresses (5.6, 12.6, 19.6, 26.6, 33.6, 40.6 MPa) with 2.8 MPa Amplitude

minor loops in the regions of saturation show very little change in the magnetization as well as very little hysteresis as is expected from observing the major loops.

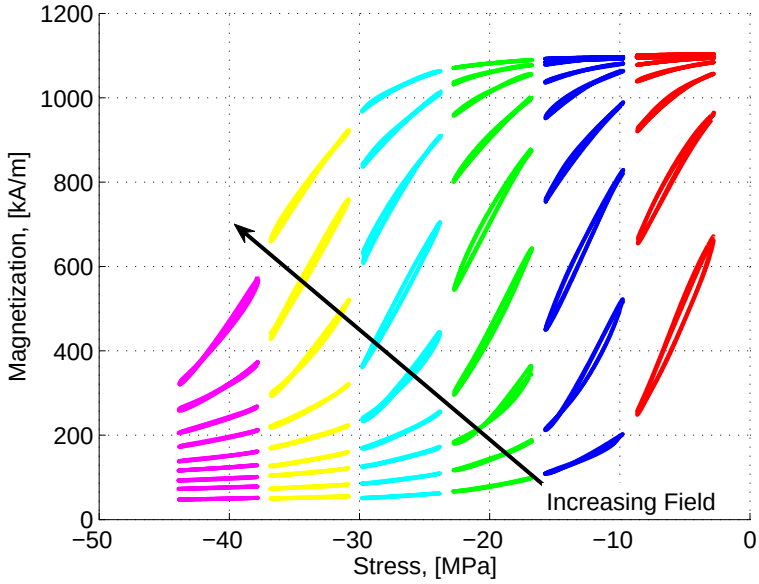

Figure 2.13: Magnetization vs. Stress for Minor Loops with Constant Field Excitation - Bias Stresses (5.6, 12.6, 19.6, 26.6, 33.6, 40.6 MPa) with 2.8 MPa Amplitude

2.4 Major and Minor Loop Comparison

One of the first observations in the comparison between the major and minor loops is that the curves about a bias point fall inside the major loops. The relationship between the major and minor loops can be seen more clearly in Figure 2.14 and Figure 2.15. The inset on these figures corresponds to the bias stress of approximately -20 MPa with the same initial bias field (4.0 kA/m). These figures highlight more clearly the difference in hysteresis between the constant current and constant field tests. It is also apparent how the minor loops follow the major loop curves in trajectory. This observation shows that operating around a bias point does not alter the general response of the system. Another observation of note in the comparison is that the minor loops are less sensitive than the major loops. There is a slight variation in

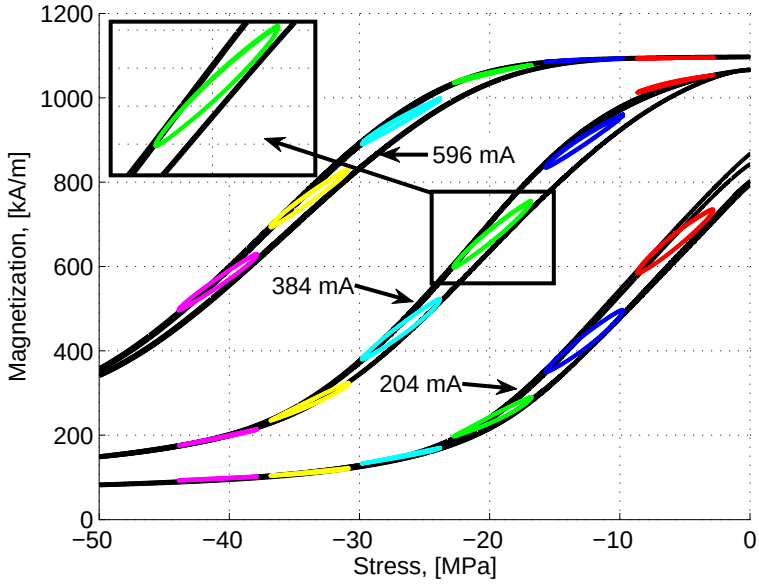

Figure 2.14: Magnetization vs. Stress for Minor and Major Loops with Constant Current Excitation

the sensitivity as the loop needs to close itself but has less range to do so. This is also a function of the input frequency which will be discussed further in the next chapter. Figure 2.16 and Figure 2.17 indicate this change in sensitivity for the three fields shown in Figure 2.14 and Figure 2.15. These sensitivities were calculated by finding the crossing point of the sensitivity for both the upper and lower portion of the loop. At this point, both the bottom and top of the curve have the same sensitivity and stress value. This sensitivity can also be approximated by fitting a first order polynomial to the entire minor loop. These figures also show the major loops for the same fields as a comparison for how the minor loops have a lower sensitivity than the major loops. The minor loops again follow the same shape of the curve; however the actual sensitivities are lower for the minor loops.

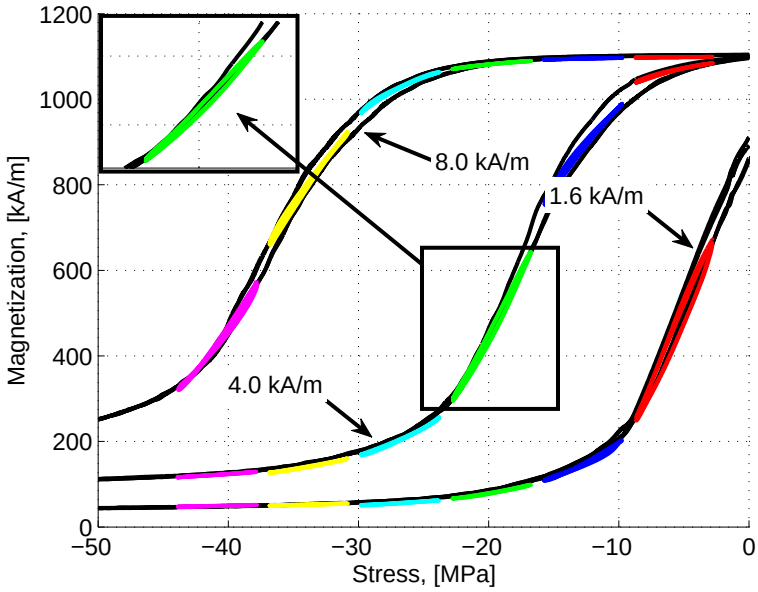

Figure 2.15: Magnetization vs. Stress for Minor and Major Loops with Constant Field Excitation

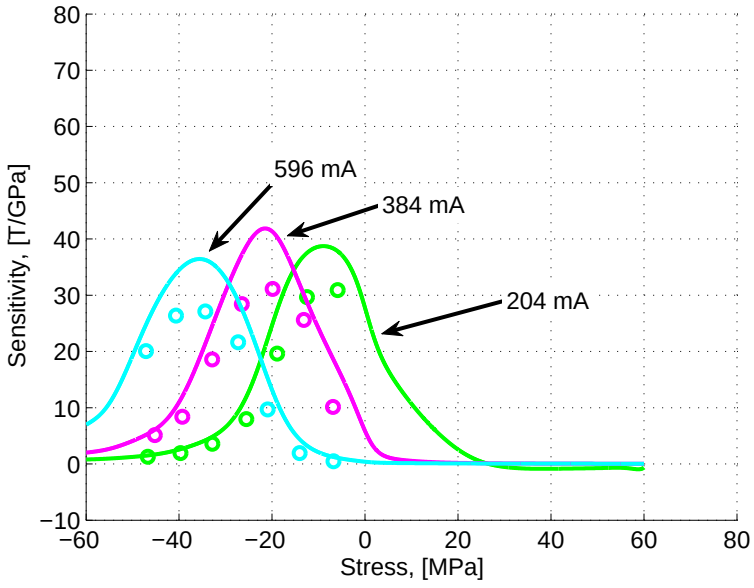

Figure 2.16: Sensitivity vs. Stress for Minor and Major Loops with Constant Current Excitation - Lines: Major Loops; Dots: Minor Loops

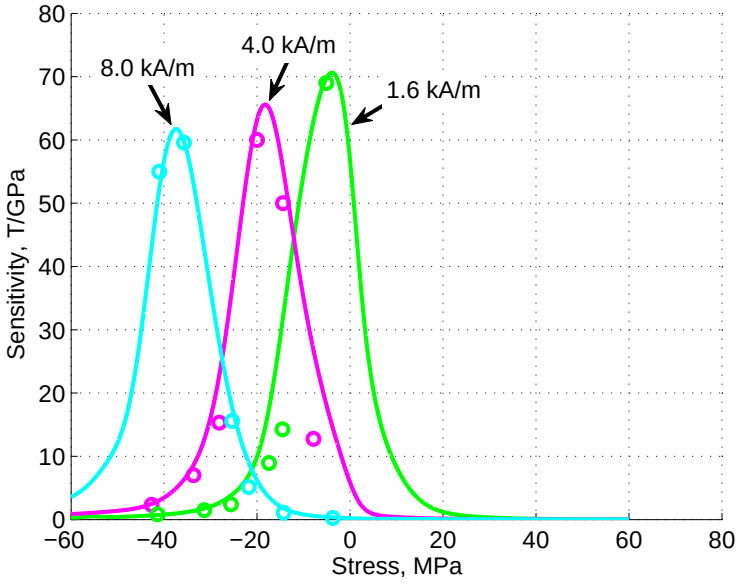

Figure 2.17: Sensitivity vs. Stress for Minor and Major Loops with Constant Field Excitation - Lines: Major Loops; Dots: Minor Loops

2.5 Summary

This chapter focused on the material characterization of a Galfenol alloy. The sensing curves for both a constant current excitation and a constant field generation were shown to highlight the differences in operation. This data can be used to determine the model parameters and aid in the future design of devices making use of this material. Minor loops were also shown to determine the behavior of Galfenol in a real world type environment. In a sensing application it would be difficult to use the entire range shown in the major loops because of the nonlinearities of the material. For this reason, using a smaller range of operation would improve the simplicity of the design. The sensitivity of the material was also calculated for both the major and minor loops. This again highlights the differences in the methods of operation as well

as defines optimal regions for operation to achieve large outputs for a given input. The next chapter will discuss how the response of Galfenol depends on the frequency of the input stress.

Chapter 3: FREQUENCY CHARACTERISTICS

3.1 Overview

The potential provided by Galfenol-based sensors leads to possible applications over a wide range of frequencies. The sensor must be able to perform at both low and high frequencies. To better understand how the frequency of the input force affects the output from the transducer, testing was done at both high and low input frequencies. Determining how the material behaves over a range of frequencies will aid in the future use of Galfenol alloys. The following chapter is divided in two sections. The first portion discusses the low frequency dependence (up to 1 Hz), while the second section discusses the higher frequency results (up to 1000 Hz). These experiments and their results are explained in the following sections.

3.2 Low Frequency Dependence

To make a robust sensor, the sensor should output a constant signal at any frequency. In this manner, any amplification of the signal will not adversely affect the signal at certain frequencies. If the signal is low at one frequency and high at another this could lead to problems with signal processing. Using an amplification to improve the signal at low frequencies could make the signal at higher frequencies too large.

This makes the sensor more difficult to use over a wide range of frequencies. Also, the output is not directly proportional to the stress input because the voltage depends on the frequency. With this approach, additional processing would be required to recover the force input that is being detected.

The main output of the Galfenol-based sensor is the voltage from the pick-up coil. A pick-up coil is wound around the center of the Galfenol sample, and produces a voltage in response to the flux density in the material. The pick-up coil is typically a small coil with a relatively few number of turns. The voltage from a pick-up coil depends on the rate of change of the flux density as seen in,

$$V = -NA\frac{dB}{dt}. \tag{3.1}$$

where V is the induced voltage, N is the number of turns, A is the cross sectional area of Galfenol, and B is the flux density in Galfenol.

This is the reason that an integrating flux meter was used in the previous chapter for the material characterization. With a constant current to the drive coils, the only mechanism that changes the flux density is the application of stress. As the frequency of this input stress decreases, the voltage from the pick-up coil also decreases. This relationship can be seen directly from the above equation because at lower frequencies, the rate of change of the flux density is also reduced. Figure 3.1 shows experimental data to further prove this theory. For this test, a 5 MPa amplitude sine wave was applied to the sample with an initial bias field of $\approx$ 1.59 kA/m to be in a region of high sensitivity. The current to the excitation coils was kept at a constant 204 mA throughout the test. The stress was applied after first reaching a bias stress of 15 MPa. This figure shows an approximately linear relationship between the frequency and the voltage output which is in agreement with Equation (3.1).

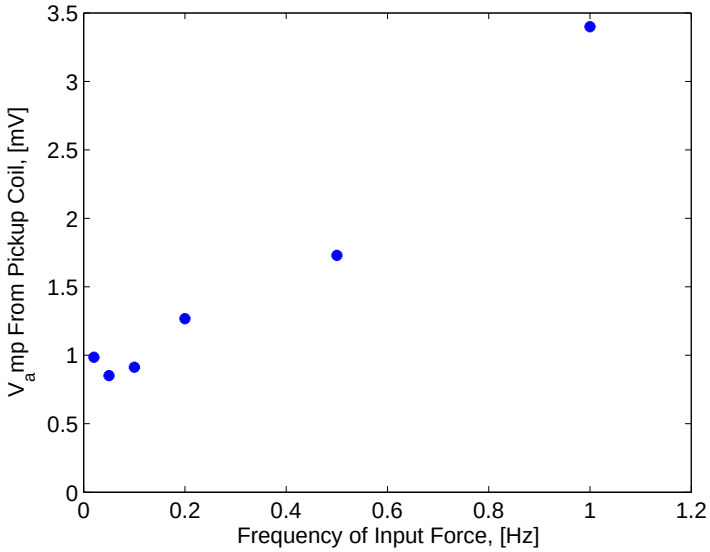

Figure 3.1: Pick-up Coil Voltage Amplitude vs. Frequency of the Input Stress Signal

3.2.1 Modulation for Low Frequencies

One method of dealing with the frequency dependent voltage amplitude is to use a modulation process. In this process, a high frequency current signal is provided to the drive coils. This creates a high frequency field signal in the sample, and thus, a continuously varying flux density. Using a higher frequency means that the signal from the pick-up coil is increased in amplitude as well. This high frequency signal is called the carrier wave. The carrier wave frequency should be much higher than that of the input stress. This allows for the high frequency carrier wave contribution to be filtered out after the demodulation process.

After applying a carrier wave to the transducer, the input stress can then be applied. The output at the flux meter is then a modulated signal combining the effects of the carrier wave and the input stress wave. For this testing, a 1000 Hz

carrier wave was selected so as to be well above the 1.0 Hz frequency that was to be the largest in this round of testing. An example of these curves can be seen in Figures 3.2, 3.3, 3.4, and 3.5. Figure 3.2 shows the carrier wave that describes the input field to the system. Figure 3.3 shows the original carrier wave from the pick-up coil (blue) as well as the modulated signal with a stress input with a frequency of 1.0 Hz (red). Demodulating the signal involves multiplying the modulated signal by the original carrier wave, and is shown in Figure 3.4.

Equations (3.2), (3.3), (3.4), and (3.5) represent this process analytically. Equations (3.2) and (3.3) represent the signal and carrier waves, respectively. In these experiments, the recorded signal is in the form of Equation (3.4) which must then be manipulated as described above to effectively obtain Equation (3.5). The signal wave is given by,

$$A_{Signal} = X_s \sin(2\pi f_s t), \tag{3.2}$$

where X_s is the amplitude and f_s is the frequency of the signal wave. The carrier wave is then given by,

$$A_{Carrier} = X_c \sin(2\pi f_c t), \tag{3.3}$$

where X_c is the amplitude and f_c is the frequency of the carrier wave. Multiplying the two together and using trigonometric identities leads to the modulated signal as expressed by,

$$A_{Modulated} = \frac{X_c X_s}{2}[\cos(2\pi(f_c - f_s)t) - \cos(2\pi(f_s + f_c)t)]. \tag{3.4}$$

The modulated signal is then multiplied again by the carrier wave to obtain the demodulated signal as given by,

$$A_{Demodulated} = \frac{X_c X_s}{4|X_c|^2}[2\sin(2\pi f_s t) + \sin(2\pi(2f_c - f_s)t) - \sin(2\pi(2f_c + f_s)t)]. \tag{3.5}$$

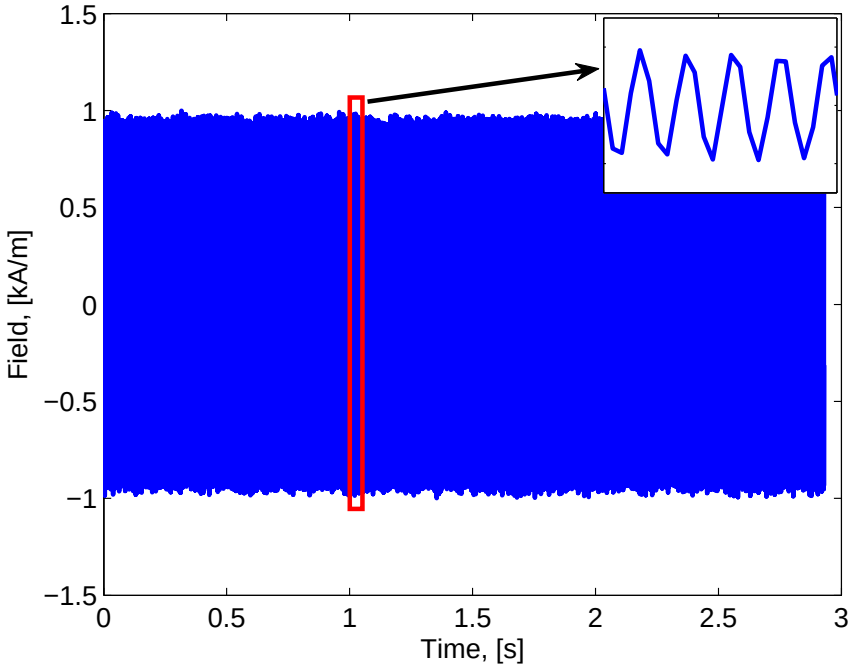

Figure 3.2: Field Carrier Wave Signal for Modulation Technique

Equation (3.5) can then be filtered to recover the portion of the signal that is due to the stress input. Figure 3.5 shows the filtered signal for the 1.0 Hz signal. The oscillations at the beginning of the signal are due to the phase lag introduced by the filter, and the fact that the mean value of the signal is not zero. A zero mean value would not have oscillations; however there would be a small portion of the signal that was flat before the signal is recovered regardless of what the actual signal was doing because of the lag of the filter.

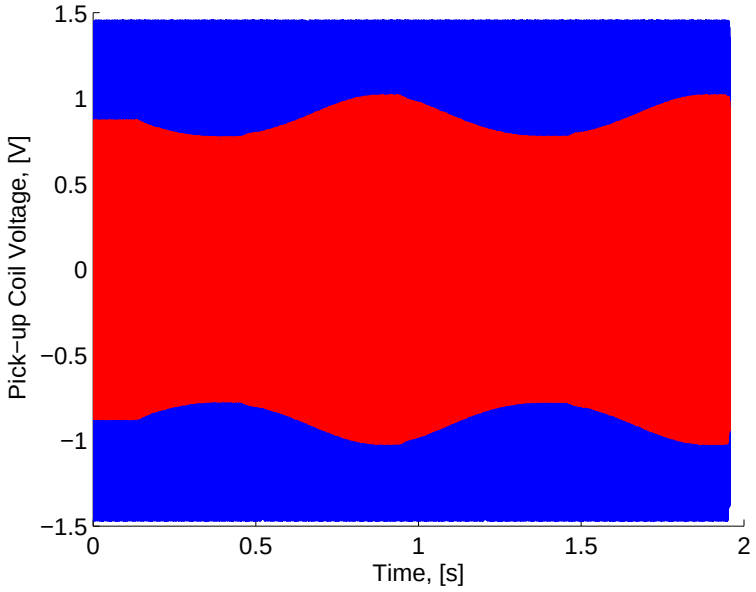

Figure 3.3: Modulated Signal and Carrier Signal from Pick-up Coil for a Input Signal with a Frequency of 1.0 Hz

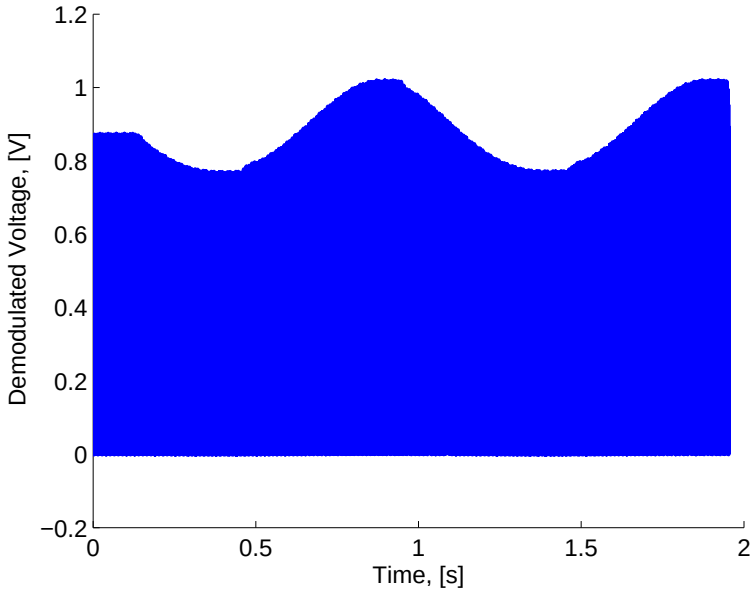

Figure 3.4: Demodulated Signal for 1.0 Hz Input Stress Signal

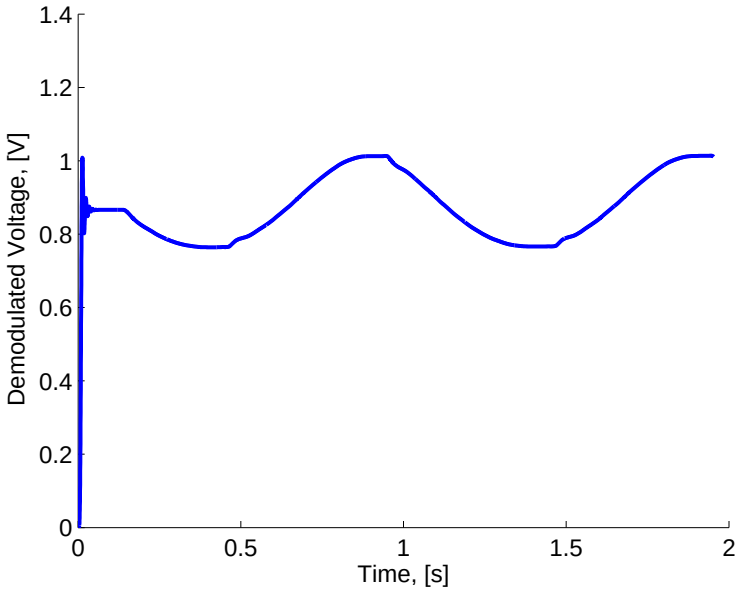

Figure 3.5: Filtered Demodulated Signal for 1.0 Hz Input Stress Signal

For this test, the same stress input as mentioned above was used at various frequencies. A 5 MPa amplitude sine wave with a mean stress of approximately 15 MPa with various frequencies was used. The modulated signal was obtained from the pick-up coil, and the result was demodulated with the known carrier wave. After the demodulation process, the resulting signal was filtered to recover the original signal. The voltage amplitude values of the demodulated and filtered signal are plotted in Figure 3.6 versus their respective input stress frequency, and it can be observed that the amplitude values are approximately constant over the range of input frequencies. The percent difference between all the tests is less than 2%. This testing has helped to validate the idea of a constant output voltage with a constant stress input. This is based on the stress-dependent susceptibility of Galfenol as described by Evans et

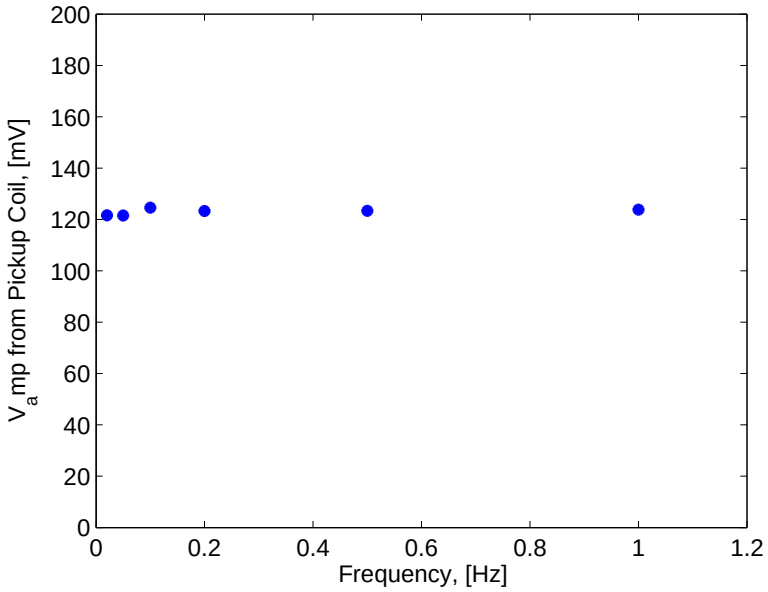

Figure 3.6: Pick-up Coil Voltage Amplitude vs. Frequency of the Input Stress Signal Using Modulation Technique

al. [14]. To further validate this concept, further testing at higher frequencies was conducted and is described in the following section.

3.3 High Frequency Characterization

Another area of interest with Galfenol-based sensors is in the application of stresses at high frequencies. The previous characterization of the materials was conducted at low or quasi-static frequencies. To fully understand how the material behaves, and thus design a better sensor, one must also look at the characterization data at higher frequencies. This section will look at the testing procedure used to accomplish this characterization, as well as the results of the testing. The first step was to look at the direct characterization involving the magnetic quantities such as flux density, field,

and corresponding load. After observing this response, the modulation process was conducted to provide further evidence of this proof of concept in a force sensor design.

3.3.1 Testing Procedure

Testing Galfenol at high frequencies is a difficult test because the material is similar in nature to other metals. This means that to get a significant change in stress, the force applied must also be large. The sample dimensions were decreased to reduce the required force input for a corresponding stress input, but the limit in this reduction is the robustness of the sample. Making the dimensions too small would lead to potential issues with buckling and bending as the load is applied.

For this testing, the same material as described in Chapter 2 was used in a dynamic set-up. The load frame can only apply force at low frequencies because of the use of a worm-gear transmission. Other load frames use hydraulics which are again limited in frequency. The dynamic set-up used in this testing makes use of two stiff supports and a cross member to create a nearly rigid structure. The Galfenol sample is connected to one support through an OMEGA LC703-1K load cell, and a piezoelectric actuator is attached to the other support. The actuator is a PSt 1000/16/80 Vs25 from AmericanPiezo, Inc.

The two supports are moved towards each other until the actuator push rod meets the end of the Galfenol sample. The supports are then secured and the cross-member affixed to "block" the Galfenol and actuator together. This enables all of the force generated in the actuator to be applied to the sample. Another limitation in this set-up is the limited deflection of the actuator used. Piezoelectric materials strain in the presence of an electric field, and are suitable for high frequencies. For this actuator,

full range of operation is achieved with a 0-1000 V signal. Piezoelectric materials behave similar to a capacitor, which means that to get the full range of operation out of the actuator, a large current is needed to operate the actuator at high frequencies. For this reason, a RCV1000/7 switching amplifier from AmericanPiezo was used.

As an electric signal is applied to the actuator, the push rod extends which causes a compression in the Galfenol. Due to the limited range of displacement from the actuator and the compliance of the other components in the system, the force in the Galfenol is limited. The stiffness of each component has a significant impact on the load applied, and in this scenario, the stiffness of the load cell plays a large role in limiting the force input. This set-up can be seen in Figure 3.7 without the cross bar. The cross bar connects the two ends and goes directly across the Galfenol sample. For clarity, a cartoon depiction of this set-up can be seen in Figure 3.8

The small range of actuator displacement limits the range of stresses that can be applied as mentioned above. To counter this problem, a pre-stress mechanism is used to first compress the sample to a bias point, and the actuator is then activated to create a high frequency stress input to the sample. The piezoelectric actuator used in this manner is always operated in compression, because the piezoelectric material is very fragile under tensile loading. The overall procedure is the same as the minor loops discussed in Chapter 2. At higher frequencies the tolerances of the pre-stress device interaction became significant and caused a kinking in the forcing signal. To get a relatively smooth set of data, the pre-stress device was removed for the results shown below. The pre-stress seen in the following section is a result of an electrical

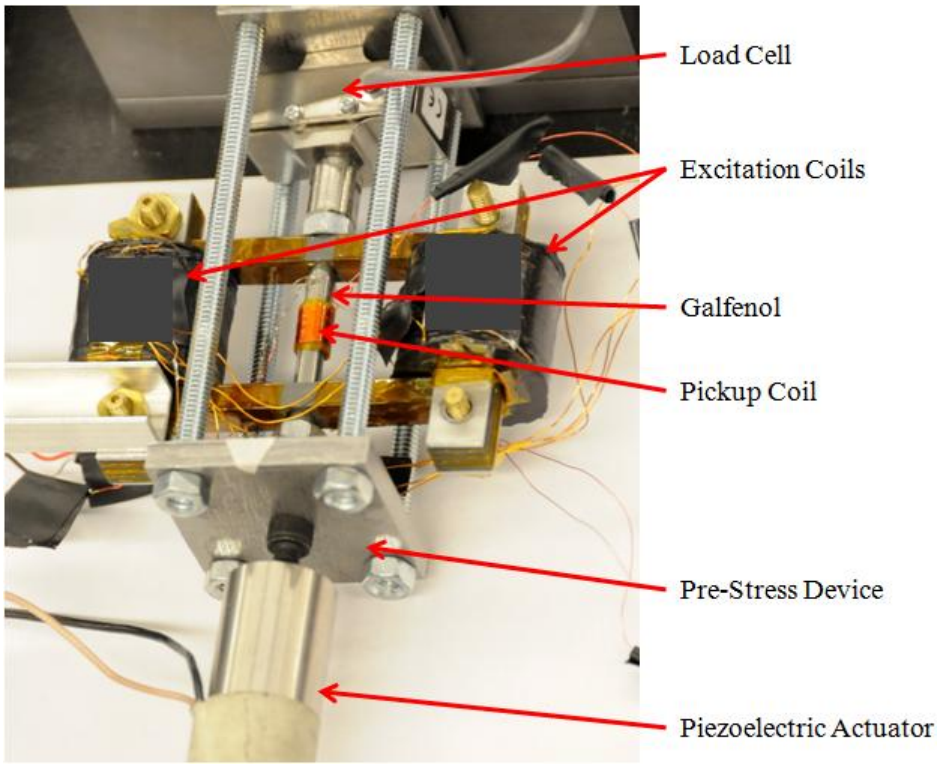

Figure 3.7: High Frequency Testing Set-up

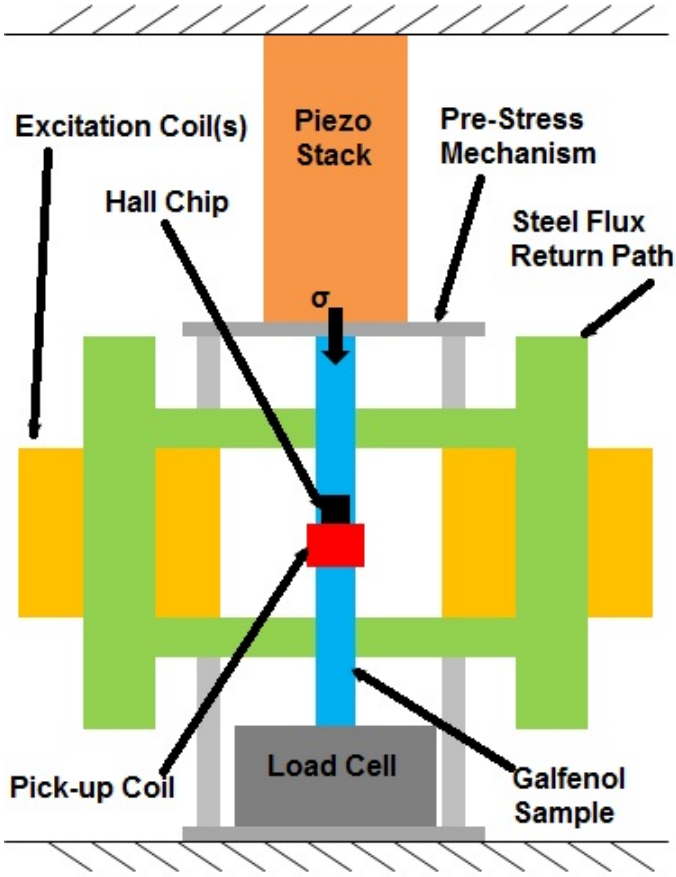

Figure 3.8: Cartoon Depiction of Dynamic Set-up

bias to the piezoelectric actuator. The results of the testing with a bias stress point of approximately -14 MPa can be found in Appendix B.

3.3.2 High Frequency Results

The results of the high frequency minor loop testing is graphed in Figure 3.9. This test was conducted with the only initial bias stress coming from an electrical offset to the piezoelectric actuator. A sinusoidal voltage was superimposed on top of this offset to produce the forcing signal that generated the minor loops seen below. For this testing, the electrical offset produced a bias stress of approximately 5 MPa, and the superimposed forcing signal had an amplitude of approximately 2.8 MPa. Due to the interaction of all of the components in the system, the forcing amplitude varied with the frequency of actuation. To have a set of curves with a consistent forcing amplitude, the voltage to the amplifier was adjusted. Through this process, the input stress amplitude of each test was kept within a 1.5% error of each other.

From these results it can be seen that the hysteresis and sensitivity change with the changing frequency. To compare the hysteresis, the area inside the curve was calculated for each frequency. The hysteresis was found by using a numerical integration procedure in MATLAB. The minor loop was split into two curves; one for increasing compressive stress and one for decreasing compressive stress. The two curves can be seen as the top and bottom curves in Figure 3.9. The top curve is generated with increasing compressive stress while the bottom curve is obtained while decreasing the compressive stress. The numerical integration of the bottom curve was subtracted from the numerical integration of the top curve to determine the area enclosed in the minor loop. This represents the hysteresis loss during the test. Figure 3.10 shows the

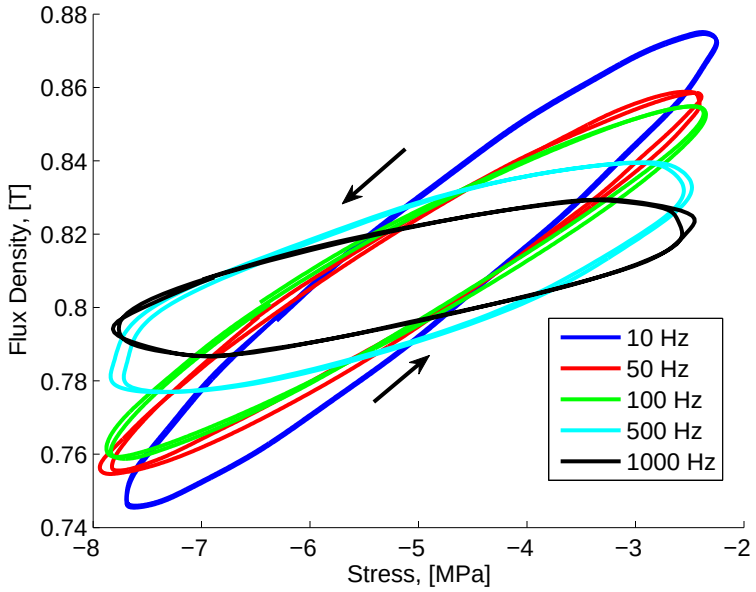

Figure 3.9: Flux Density versus Stress for Five Frequencies (10 Hz, 50 Hz, 100 Hz, 500 Hz, 1000 Hz) with Initial Bias Field: 1.6 kA/m (204 mA); Bias Stress: 5 Mpa; Stress Amplitude: 2.8 MPa

hysteresis as a function of the input forcing frequency. There is a kink at 50 Hz and then the hysteresis increases until 500 Hz when the hysteresis begins to decrease once again. This kink will be discussed later in this section.

The sensitivity is compared by looking at the anhysteretic response at each frequency. The slope of this curve was then calculated by fitting a linear line to the entire minor loop. The slope of this line was used as a comparison of the sensitivity for each curve. Figure 3.11 shows the sensitivity as a function of the input forcing frequency. Here it can be seen that the sensitivity decreases more rapidly at lower frequencies, and the decrease becomes more gradual as the frequency increases. This change in sensitivity is an undesirable characteristic for sensing.

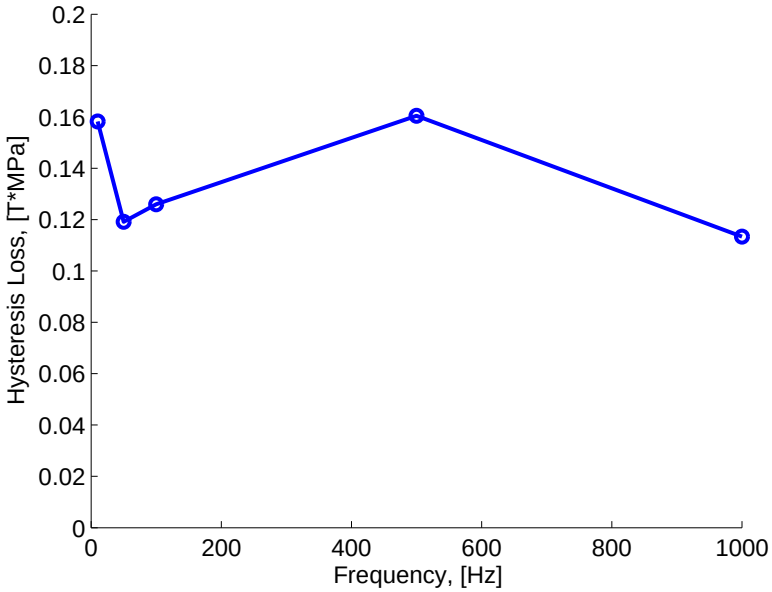

Figure 3.10: Hysteresis versus Frequency of Input Stress Signal

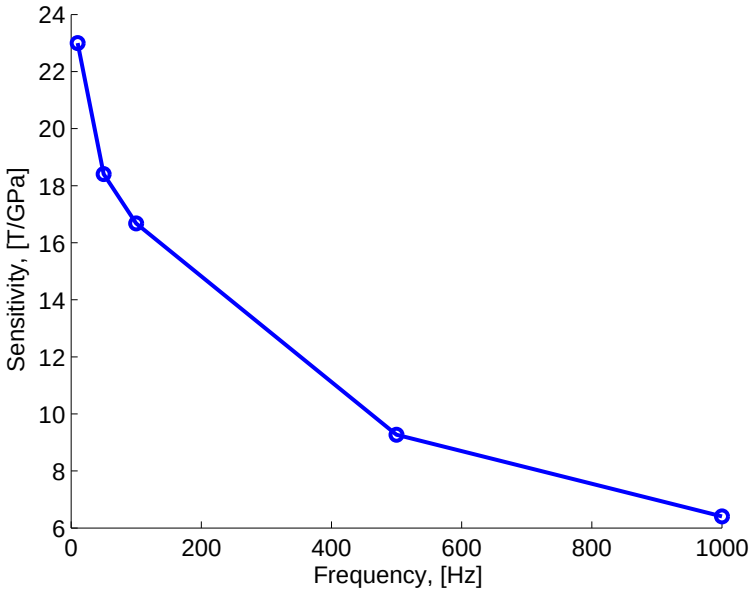

Figure 3.11: Sensitivity versus Frequency of Input Stress Signal

To gain a better understanding of how the material behaves over a broad range of frequencies, a stepped sine test was conducted with the same set-up as described above. For this test, the amplitude of the forcing signal was kept to approximately 1.4 MPa (10 lbf) through a controller inside the software so as to have a equivalent comparison. A Quattro Data Acquisition was used to generate the stepped sine input as well as collect the data. The frequencies observed were from 1 Hz to 1000 Hz in three distinct bands. For the range from 1 Hz to 10 Hz, the spacing was set to 1 Hz, 5 Hz spacing from 10 Hz to 100 Hz, and 10 Hz spacing from 100 Hz to 1000 Hz. In this manner, there is more spacing at higher frequencies because at higher frequencies, the actuator tends to heat up.

To avoid damage to the actuator, high frequency testing must be kept short. Also, by keeping the force input low, the actuator does not require the full range of input voltage, which means it draws less power, and therefore heats up slower. During the stepped sine test, the amplitude of the flux density was recorded as a transfer function over the input force. Figure 3.12 shows the results of this test. The top part of Figure 3.12 shows how the magnitude of the flux density over the amplitude of force decreases with an increasing frequency. The bottom portion of Figure 3.12 shows the phase angle of the transfer function. This plot shows that the angle of the response between 10 Hz and 100 Hz has a small bump. This is a large contributing factor to the kink that was seen in the hysteresis plot shown earlier. The results from the stepped sine test agree quite well with those obtained at discrete frequencies. A comparison of these two types of data can be found in Appendix B.

To further understand the frequency response of the system, the above testing was expanded to larger frequencies. The testing was conducted from 10 Hz to 10 kHz. The

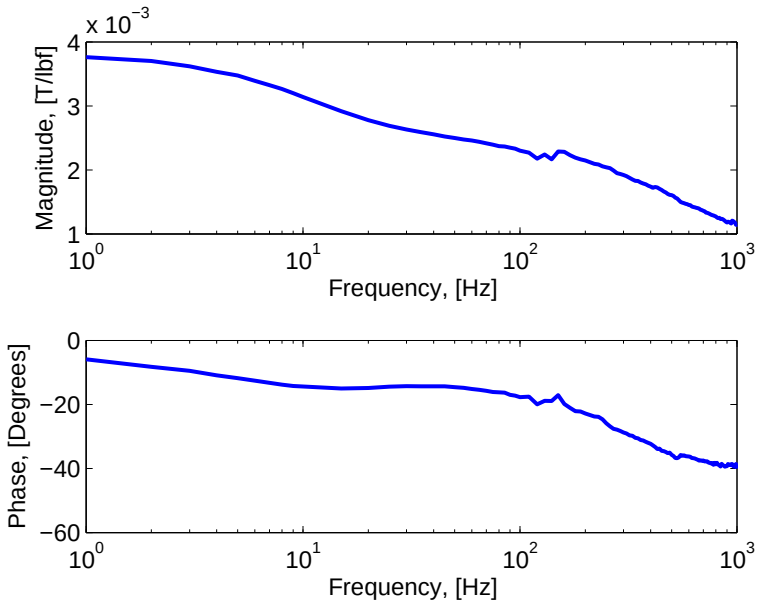

Figure 3.12: Magnitude and Phase Response of Galfenol With a Sine Input of Amplitude 1.4 MPa, Bias Stress Point of 5 MPa and Initial Bias Field of 1.6 kA/m (204 mA)

same set-up was used with the stress input reduced to 0.7 MPa to keep the actuator in the safe limits of operation. The results of this test are shown below in Figure 3.13. The results show a resonance and anti-resonance pair around 6 kHz. This resonance and anti-resonance pair is common in magnetostrictive materials. Also, the slope of the overall response in this region is approximately -20 dB/decade which relates to the fact that there is a first order relationship between the magnetic and mechanical regimes. Also shown in Figure 3.13 is the comparison with the first test which shows good agreement and shows how the first test up to 1 kHz was operating in the stiffness controlled region and shows a slight decrease but overall stays relatively flat in comparison to the overall frequency response shown in blue. It should also be noted that the anti-resonance at approximately 10 kHz is due to the resonant

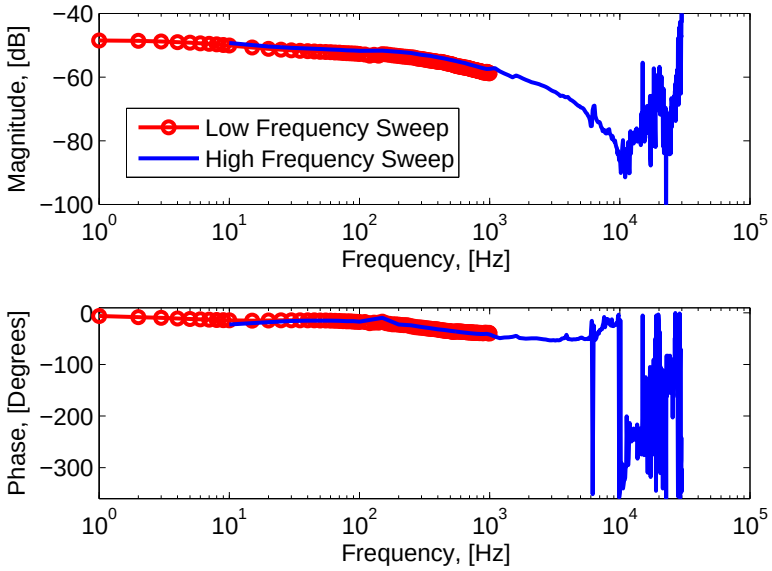

Figure 3.13: Magnitude and Phase Response of Galfenol With a Sine Input of Amplitude 0.7 MPa, Bias Stress Point of 5 MPa and Initial Bias Field of 1.6 kA/m (204 mA)

frequency of the entire system. Also, the anti-resonance at approximately 23 kHz is due to the resonance of the piezoelectric actuator itself.

An additional test was conducted to look at the impedance of the system under two different conditions. The free conditions showed a resonance and anti-resonance pair at approximately 19 kHz. This is shown below in Figure 3.14. This test was conducted by sweeping the frequency of the input to the excitation coils while monitoring the pickup coil voltage as well as the current in the excitation coils. A similar test was conducted by first loading the sample with the piezoelectric actuator in the same manner as the above frequency response and then sweeping the excitation coil

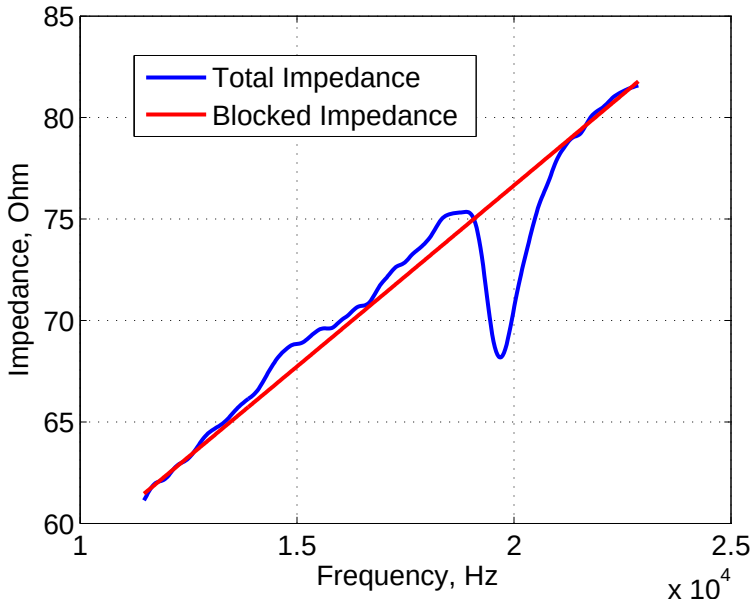

Figure 3.14: Impedance Measurement of Transducer with No Loading

frequency rather than the input frequency to the actuator. The pick-up coil voltage and excitation current were measured and the transfer function of voltage over current is shown in Figure 3.15. This shows a resonance and anti-resonance pair at approximately 4 kHz. This is close to the 6 kHz shown in the above figure with some variation due to differences in the loading and the different method of excitation.

The change in amplitude and phase angle are due to the response of the magnetic domains to the applied stress. This material has a large anisotropy energy which limits domain rotation, so the magnetization process is dominated by domain wall motion. In this process, the domains nearest to the direction of the applied field grow in consequence to those in other directions. In this manner, the material becomes magnetized along the direction of the applied field. During the higher frequency

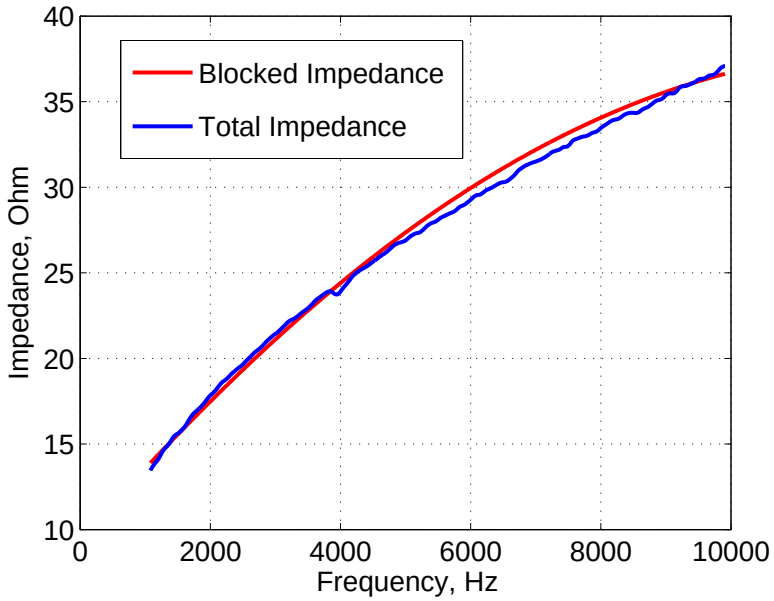

Figure 3.15: Impedance Measurement of Transducer with Initial Stress of Approximately 5 MPa

testing, this domain wall motion occurs, but as the frequency increases the domains have less time to grow or shrink. As the stress changes directions rapidly, the domains must grow and shrink accordingly. With a limited amount of time, the domains cannot grow as much as they would under quasi-static loading and thus the amplitude decreases. Also, the phase lag is a result of the domains changing their growth directions rapidly and ultimately lagging behind the forcing signal input.

3.3.3 Modulation for High Frequencies

To further understand the behavior of the material a similar modulation technique to that used for the low frequency characterization, was used. The sample of Galfenol was loaded into the high frequency set-up as described above. This set-up allowed a mechanical pre-stress to be imposed on the material and the forcing signal to be

superimposed from that point. For this experiment, to test the same frequencies as tested in the generic high frequency testing, a carrier wave of 5 kHz was chosen. This frequency was high enough so that during the filtering process the original signal could be recovered.

The carrier wave was set such that the field was a constant amplitude of approximately 1 kA/m in the original pre-stressed state. The forcing signal was then superimposed on the carrier wave and the resulting modulated voltage from the pickup coil was recorded. Using the known carrier wave, the signal could then be demodulated and filtered to recover the original signal. As with the other high frequency testing, there was a kink in the forcing signal, and the forcing amplitude was not controlled. These results are shown in Appendix B. To create a truly equal comparison, the mechanical pre-stress was once again removed, and the test was conducted with an electrical bias to the piezo. The electrical bias produced a bias stress of approximately 5 MPa, and the voltage amplitude to the actuator was adjusted at each frequency to keep the stress amplitude at 2.8 MPa (20 lbf) as in the previous high frequency tests.

The process is similar to that as used in the low frequency modulation with the exception being the frequency of the carrier wave. For the high frequency modulation, a 5 kHz carrier wave was used. One of the quantities of interest in this testing is the amplitude of the voltage with respect the frequency of the forcing signal. This is shown in Figure 3.16. It can be observed that the voltage response of the pick-up coil is approximately flat over the range of frequencies. This means that the output voltage using the modulated technique does not depend on the frequency of the forcing signal. Table 3.1 shows the voltage level at each frequency. As with low frequencies, this is a desirable characteristic of a force sensor utilizing Galfenol because it allows

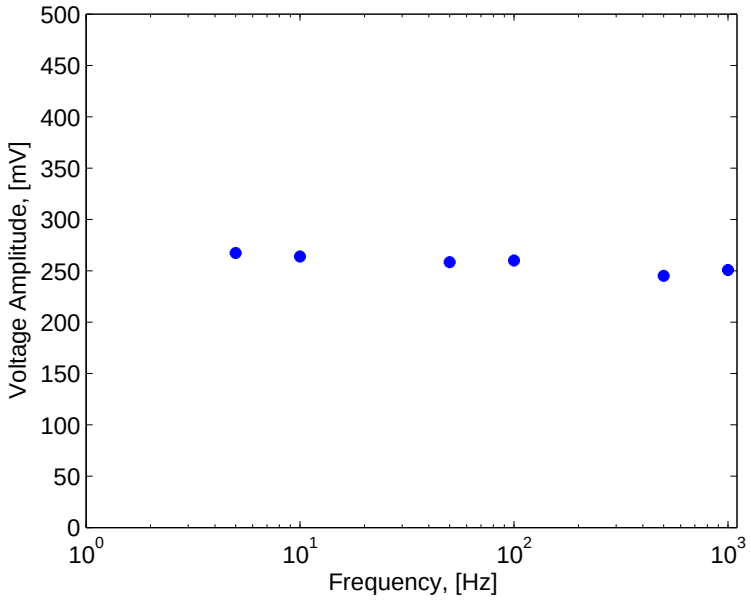

Figure 3.16: Pick-up Coil Output Voltage vs. Frequency of Input Stress Signal

for a common gain to be used. This flat response is in contrast to the previous high frequency testing where the sensitivity decreased with the increasing frequency of stress input. This is one of the main advantages to using the modulation technique for a Galfenol based force sensor.

Table 3.1: Voltage Amplitude at Each Frequency of Stress Input

Frequency [Hz]	Voltage Amplitude [mV]
5	267
10	264
50	259
100	260
500	245
1000	250

An additional point of interest with regards to the modulation technique is the response to a step input. This test was conducted in a similar way to that of the previous testing at different frequencies except that the input to the actuator was a step in voltage, and thus a step stress input to the material. Using this procedure, a step input of approximately 2.86 MPa (20 lbf) was generated. For this test, the voltage change after demodulation was 230 mV. The modulated and demodulated and filtered signal for the step input can be seen in Figure 3.17 and Figure 3.18 respectively.

While the stress amplitude was adjusted to be approximately equal over the range of frequencies, there was still some variation. For this reason an even better comparison for the sensor response over the range of frequencies is to look at the voltage per unit input force. Table 3.2 shows these values for the different frequencies and the step input.

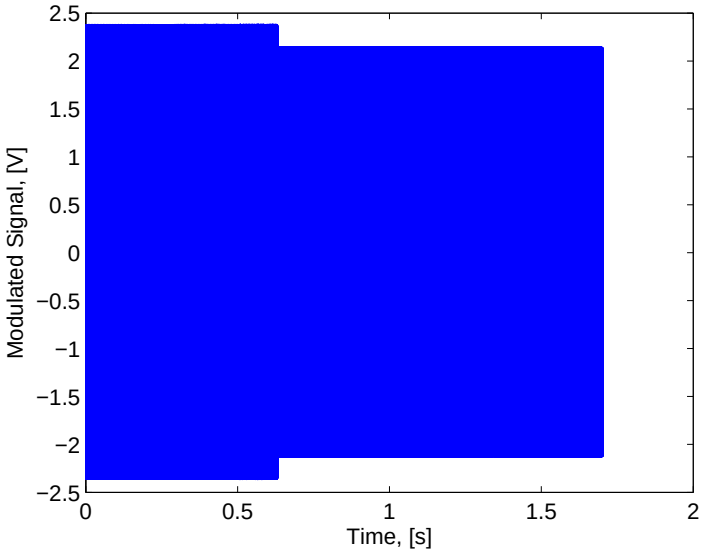

Figure 3.17: Modulated Signal for a Step Input

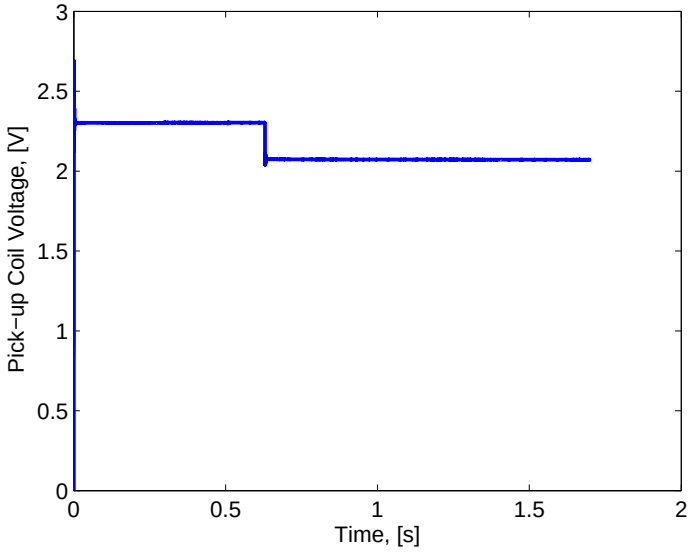

Figure 3.18: Demodulated and Filtered Signal for a Step Input

Table 3.2: Voltage Per Unit Input Force at Each Input

Input	Voltage per Unit Input Force [mV/N]
5 Hz	2.97
10 Hz	2.99
50 Hz	2.92
100 Hz	3.02
500 Hz	2.76
1000 Hz	2.79
Step	2.56

Carrier Frequency

The choice of the carrier wave frequency is a key component to the analysis using the modulation technique. From (3.5) one can see that the carrier wave must be considerably higher than the signal frequency so that the filter can accurately filter out the higher frequencies to recover the original signal. The choice of carrier wave frequency is based on the highest expected signal as well as the performance of the filter. It is recommended that the carrier wave frequency is at least five to ten times larger than the largest expected frequency [13]. Modulation is common in LVDT sensors and the carrier wave is typically ten times larger than the largest signal frequency. The choice of carrier wave frequency will affect the amount of ripple as well as the delay of the filter. The type of filter used also affects the performance of the modulation technique. As an example, one can look at a scenario where the highest expected frequency is 1 khz, and the carrier wave frequency is 10 kHz. This means that the two frequencies that need to be filtered out are 19 kHz and 21 kHz. Using a simple RC filter with one resistor and one capacitor and assuming that the desired "ripple" above 19 khz is 5%, the filter will have a amplitude ratio at 1 khz of

0.68. This expression for this filter is given by,

$$\frac{V_{out}}{V_{in}}(i\omega) = \frac{1}{i\omega RC + 1} \tag{3.6}$$

where R is the resistance and C is the capacitance of the standard low-pass filter circuit. Using a more selective filter designed with two RC pairs the amplitude ratio is improved to 0.94. This type of filter is approximated by,

$$\frac{V_{out}}{V_{in}}(i\omega) \approx \frac{1}{(i\omega RC + 1)^2} \tag{3.7}$$

In comparison, if the same filter is used with a 5 kHz carrier wave the amplitude ratio is reduced to 0.81. From these relationships it is apparent that a higher carrier wave frequency improves the accuracy of the modulation technique. While improved accuracy is a desired characteristic, the next chapter will discuss potential problems with using a high carrier wave frequency for this set-up.

3.4 Summary

This chapter examined the frequency response of Galfenol through several different kinds of testing. The low frequency dependence proved the theory of frequency dependence looking at just the output of the pick-up coil with a constant current excitation. The modulation technique improved the response of the Galfenol based transducer by creating a more or less flat response with regards to frequency. This same technique was also used at high frequencies with similar results. The high frequency modulation shows a relatively flat response over a wide range of frequencies, and even including a step input. The high frequency characterization demonstrates the need for this modulation technique through showing the response of Galfenol over a broad range of frequencies with a constant current excitation. The results of

the high frequency characterization were analyzed for both sensitivity and hysteresis. This outcome showed a degradation in the sensitivity with increasing frequency as well as a nonlinear change in the hysteresis. Both characteristics would require attention for devices making use of Galfenol.

Chapter 4: POWER CONSUMPTION

4.1 Overview

As mentioned in Chapter 3, the modulation technique relies on the fact that the carrier signal is at a much higher frequency than the forcing signal. In the case of the high frequency testing done as part of this thesis, the highest frequency of excitation is 1 kHz. To get good results, the modulation frequency should be at least 5 kHz, if not higher depending on the filter used. The problems this poses is in the power requirements for the sensor. Since the way that the high frequency field is generated is through two coils and a steel flux return path, the voltage required to operate at higher frequencies becomes rather large. This is because coils act as inductors and thus to keep a constant current over a range of frequencies the voltage must also increase. Another issue is that the current required to generate the desired field is not constant over the range of frequencies due to eddy current losses in the sample and the steel flux return path. The steel flux return path is made of steel laminates to reduce this effect, but the material is not laminated. This chapter will look at the current power requirements as well as potential ways to reduce them.

4.2 Test Set-up

In the current transducer, there are two coils used to generate the field in the sample. These coils each have 1600 turns and are quite large so that the material can be saturated with a relatively low current. The main issue with this is that the larger coils have a larger inductance, and thus, require a higher voltage. To better characterize the current power requirements and the current requirements to obtain the desired field amplitude of 1 kA/m, a stepped sine test was done keeping the current to the coils small to that the amplifier could still provide adequate voltage at high frequencies. A fluke i30s current clamp was clamped around the wire leading to the excitation coils while a Techron 5050 Amplifier was used to apply a voltage to the coils. The voltage was recorded using the voltage monitor on the amplifier. The field was also measured using the same Allegro A1322LUA-T hall chip. The transfer functions for voltage and field were related to the current, and then using the inverse of the field transfer function, it was possible to determine the current, and thus, the voltage required to achieve a certain field. This testing was done under zero loading conditions.

Figure 4.1 and Figure 4.2 shows the current and voltage amplitudes needed to achieve a field amplitude of 1 kA/m in the sample. There is more noise in the signal at higher frequencies because the field was reduced as a by product of keeping the current constant. This meant that the noise is amplified at larger frequencies. The voltage was found by looking at the measured impedance of the coils relating the voltage to the current. This impedance is seen in Figure 4.3.

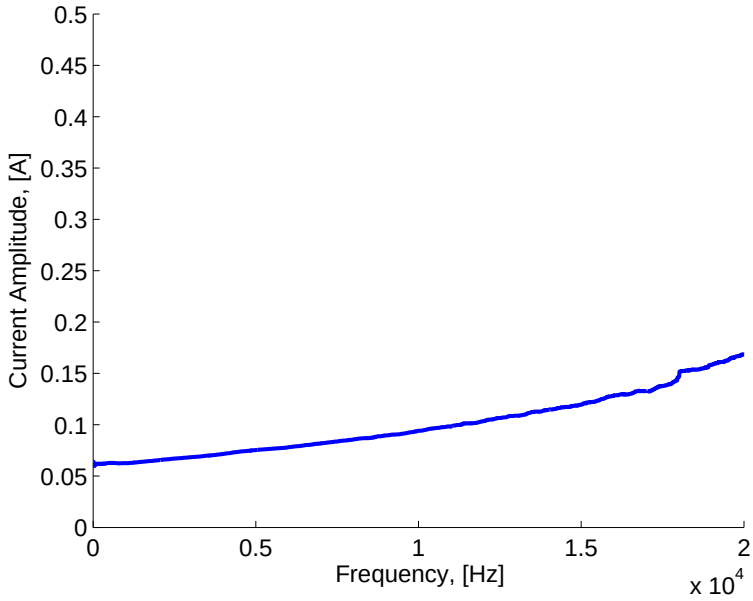

Figure 4.1: Current Amplitude Necessary to Generate a 1 kA/m Amplitude Field in Galfenol Sample

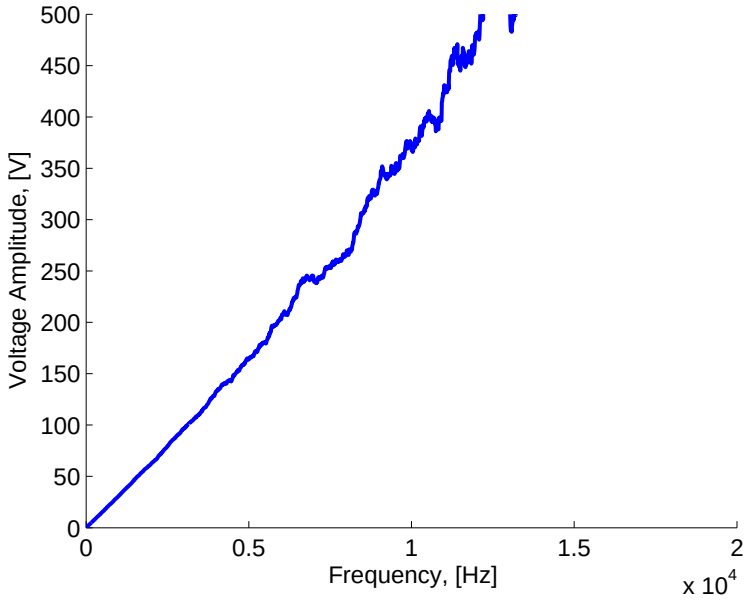

Figure 4.2: Voltage Amplitude Necessary to Generate a 1 kA/m Amplitude Field in Galfenol Sample

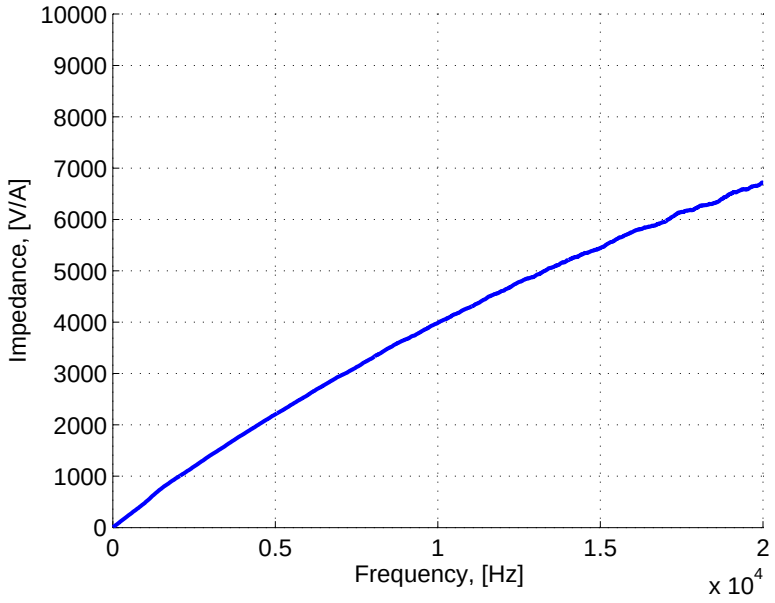

Figure 4.3: Impedance of Input Excitation Coils

From the impedance measurement it can be observed that the coils are not only inductors, but also have some capacitance which causes the curvature. This capacitance is caused by the spacing of the different turns in the coils as well as the insulation on the wires [8]. The capacitance increases approximately linearly with the number of turns, and has a jump when a new layer begins. Each layer causes a jump in the capacitance because it aids in the interaction of non-adjacent turns. The overall capacitance acts in parallel to the inductance of the coil and creates a resonance in the system. This further increases the impedance and makes the coils behave less predictably.

4.3 Current Power Requirements

Using the voltage and current calculated from the transfer functions, the peak-to-peak power can be computed. The peak-to-peak power is computed by multiplying the amplitude of the voltage and current together. The actual power signal will be affected by the phase angle between the current and voltage, but comparing the peak-to-peak power provides an equal comparison. In using this approach, the power requirements are calculated and displayed in Figure 4.4. The actual power requirements from the high frequency modulation testing is shown in Figure 4.5. This figure was computed by multiplying the voltage signal with the current signal. The mean values of both the voltage and current are approximately zero, while the power's mean value is not. This is due to the influence of the phase angle between the current and the voltage. A phase angle of zero would correspond to a mean value of half the peak-to-peak voltage and a phase angle of ninety degrees corresponds to a mean power value of zero watts. This figure shows a peak-to-peak voltage of approximately 15 W which compares well with the 12.4 W peak-to-peak value obtained by the transfer function at 5 kHz. The mean value from the modulation testing was 2.2 W.

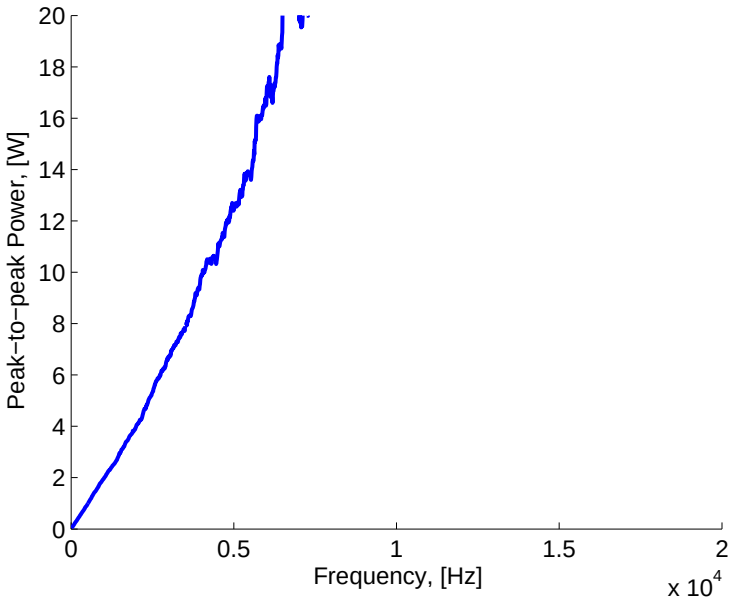

Figure 4.4: Peak-to-peak Power Necessary to Generate a 1 kA/m Amplitude Field in Galfenol Sample

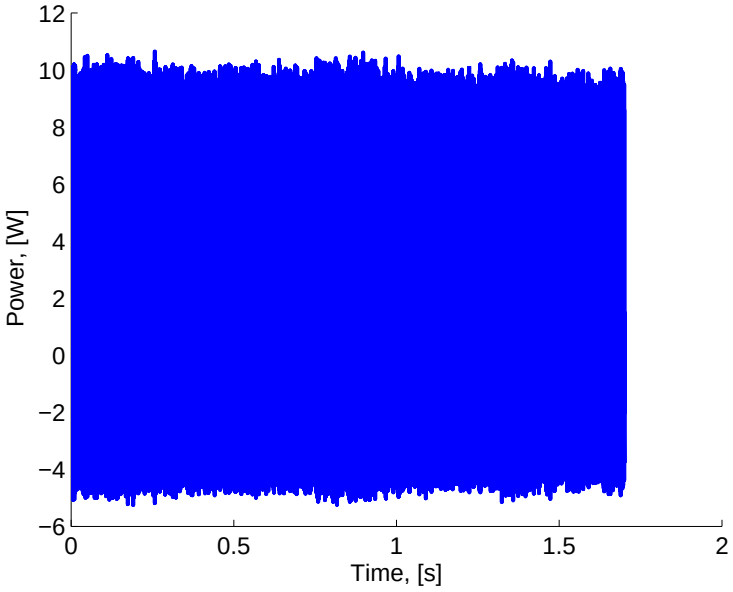

Figure 4.5: Power Signal from High Frequency Modulation Testing with 5 kHz Carrier Wave

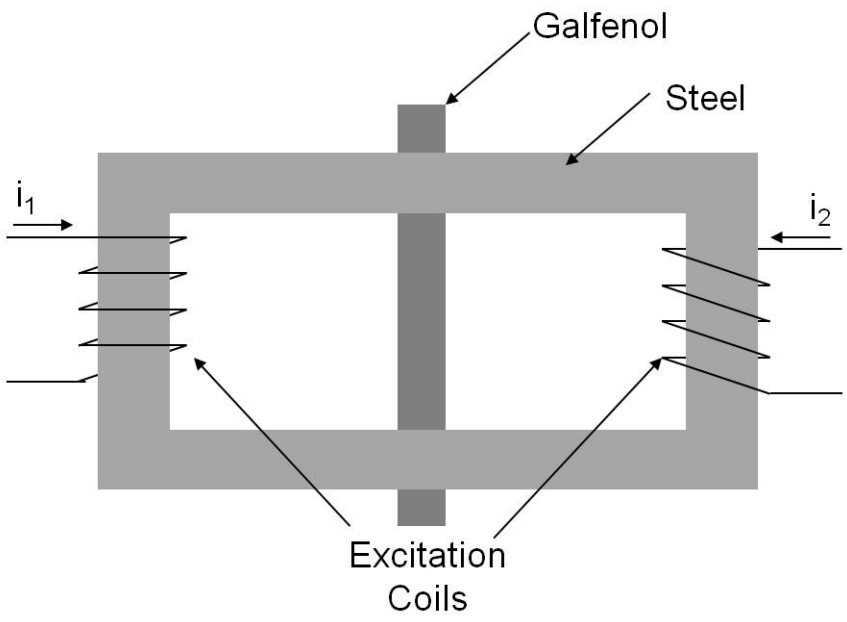

Figure 4.6: Cartoon Depiction of Magnetic Circuit Used in Experiments

4.4 Improving Power Requirements

To improve the power requirements for the transducer described it is helpful to understand the factors that affect the electrical response of the system. The main component of the electrical system is the two excitation coils, so the main factor affecting the power is the inductance of the coils. The inductance of the coils is dependent on not only the geometry of the coils, but also the geometry and construction of the magnetic circuit. Figure 4.6 shows a cartoon depiction of the magnetic circuit and Figure 4.7 shows an equivalent electrical circuit where the voltage represents the magnetomotive force, $\mathcal{F} = Ni$, and the resistors represent the reluctance of the different components of the system. The current is representative of the flux flowing in the system.

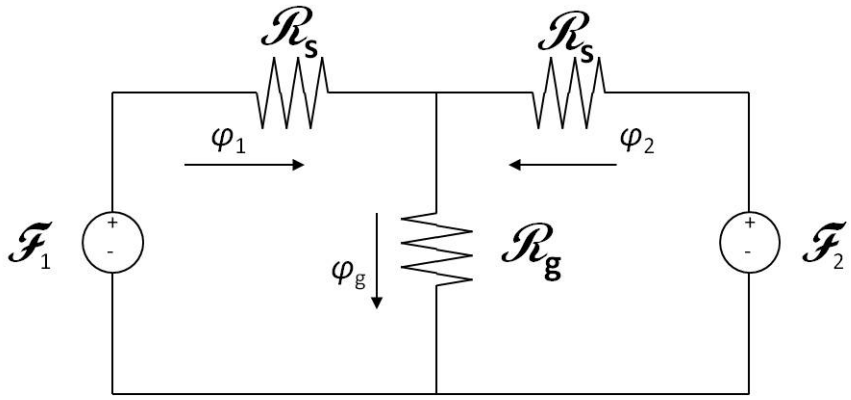

Figure 4.7: Electrical Representation of Magnetic Circuit

Using Kirchoff's voltage law one can look at both loops of the system to see that,

$$\mathcal{F}_1 - \mathcal{R}_s\phi_1 - \mathcal{R}_g\phi_g = 0, \tag{4.1}$$

and

$$\mathcal{F}_2 - \mathcal{R}_s\phi_2 - \mathcal{R}_g\phi_g = 0. \tag{4.2}$$

it can be noted that the flux in Galfenol is the sum of the flux generated in each coil. If the coils are assumed to be identical, this leads to,

$$\mathcal{F}_1 - \frac{\mathcal{R}_s\phi_g}{2} - \mathcal{R}_g\phi_g = 0. \tag{4.3}$$

This can then be solved for the flux in Galfenol as,

$$\phi_g = \frac{2Ni}{\mathcal{R}_s + 2\mathcal{R}_g}. \tag{4.4}$$

Using this flux, the field can be calculated as,

$$H = \frac{\phi}{A\mu_r\mu_0} = \frac{2Ni}{A_g\mu_r\mu_0(\mathcal{R}_s + 2\mathcal{R}_g)}. \tag{4.5}$$

The next step in determining the inductance of the coils is to look at the coupling between the mechanical and magnetic domains. This is difficult because of the non-linear behavior of Galfenol; however by using the linearized piezomagnetic equations, the analysis can be simplified. The piezomagnetic equations are tensor equations involving a full three dimensional analysis. For this analysis the interest is in one direction, and thus a one-dimensional analysis is performed. Rather than use the entire tensor, the following analysis uses just the 33 direction. As an example, instead of using the entire stress tensor, $\mathbf{T}$, only the T_3 component is used. For further simplicity this will be referred to as simply, T. The same is true for the other values where the strain, flux, and field tensors all have six components and only the third is used. The factors multiplying the inputs in fact form a six by six matrix where the quantity of interest is in the 33 position. This implies that rather than use the entire compliance tensor, $\mathbf{s}^B$, only the s^B_{33} is of interest. This is also true for both the λ and the μ^S tensors. As with the input quantities, the 33 subindex is removed in this analysis for simplicity and clarity. These linear equations are given with stress and field as the inputs and strain and flux as the outputs, but the inverse relationships are of greater interest in this analysis. The inverse relationships are given as,

$$T = \frac{S}{s^B} - \lambda B, \tag{4.6}$$

$$H = -\lambda S + \frac{1}{\mu^S} B, \tag{4.7}$$

where s^B is the compliance at constant induction, and μ^S is the magnetic permeability at constant strain. The λ term is defined by,

$$\lambda = \frac{d}{s^B \mu^T} = \frac{d}{s^H \mu^S}, \tag{4.8}$$

where the B and T represent constant induction and constant stress, and the H and S are constant field and constant strain. The relationships between the different conditions are given as,

$$\mu^S = \mu^T(1 - k^2), \tag{4.9}$$

$$s^B = s^H(1 - k^2), \tag{4.10}$$

where k is given as,

$$k^2 = \frac{d^2}{s^H \mu^T}, \tag{4.11}$$

With these relationships it is possible to relate the force and field to strain and magnetic induction. It can be noted that the force in the sample is a product of the stress and the area. Due to the fact that the equations assume a compressive stress this is a negative relationship so that,

$$F = -TA_g = -\frac{A_g}{s^B}\left(\frac{v_2 - v_1}{j\omega l_g}\right) + \lambda A_g B, \tag{4.12}$$

where the strain is given as,

$$S = \left(\frac{v_2 - v_1}{j\omega l_g}\right). \tag{4.13}$$

At this point it should also be noted that the compliance is related to the stiffness, c, through an inverse relationship. This relationship is shown as,

$$\begin{aligned} \frac{1}{c^B} &= \frac{A_g}{s^B l_g}, \\ \frac{1}{c^H} &= \frac{A_g}{s^H l_g}. \end{aligned} \tag{4.14}$$

The flux density can also be solved from (4.7) and thus giving the equation for force as,

$$\begin{aligned} F &= -\frac{v_2 - v_1}{j\omega l_g c^B} + \frac{d}{s^H \mu^S} A_g \left(H + \frac{d}{s^H \mu^S} \frac{v_2 - v_1}{j\omega l_g} \right) \mu^S, \\ &= -\frac{v_2 - v_1}{j\omega l_g c^B} \left(1 - \frac{d^2 c^B}{(s^H \mu^S)^2} \frac{A_g \mu^S}{l_g} \right) + \frac{dA_g}{s^H} H, \\ &= -\frac{v_2 - v_1}{j\omega l_g c^B} (1 - k^2) + \frac{dA_g}{s^H} \left(\frac{2Ni}{A_g \mu^S (\mathcal{R}_s + 2\mathcal{R}_g)} \right), \\ &= -\frac{v_2 - v_1}{j\omega l_g c^H} + \frac{d}{s^H} \left(\frac{2Ni}{\mu^S (\mathcal{R}_s + 2\mathcal{R}_g)} \right). \end{aligned} \tag{4.15}$$

Now the force is a function of the strain and the current in the coils. The next step is to look at the field in the material and relate that to the voltage in the coils. The field equation is given as,

$$H = \frac{2Ni}{A_g \mu^S (\mathcal{R}_s + 2\mathcal{R}_g)} = -\frac{d}{s^H u^S} \left(\frac{v_2 - v_1}{j\omega l_g} \right) + \frac{1}{\mu^S} B, \tag{4.16}$$

The flux density generated by the coils is,

$$B = \frac{V}{j\omega N A_{coil}}. \tag{4.17}$$

The flux in Galfenol is the sum of the flux from both coils such that,

$$\begin{aligned} \phi_1 + \phi_2 &= \phi_g, \\ B_1 A_{coil} + B_2 A_{coil} &= B_g A_g. \end{aligned} \tag{4.18}$$

Since the excitation coils are identical, the flux in Galfenol can be given as,

$$B_g = \frac{2V}{j\omega N A_g} \tag{4.19}$$

This can then be solved for the voltage to the coils. After solving for the voltage and simplifying, the voltage is shown to be,

$$V = \frac{j\omega N^2 i}{\mathcal{R}_s + 2\mathcal{R}_g} + \frac{dN}{2c^H} (v_2 - v_1). \tag{4.20}$$

From this equation it is evident that if the Galfenol is blocked (i.e. no strain), the inductance of the coil is given as,

$$L^S = \frac{N^2}{\mathcal{R}_s + 2\mathcal{R}_g}. \tag{4.21}$$

The value for blocked inductance can also be found in [23], where the inductance of a coil in a circuit is found by looking at both the self and mutual inductance of the coils. There is a voltage induced in the second coil from the flux generated in the first coil. Due to the fact that the flux generated in each coil are traveling in the same direction, the voltage induced in the second coil is in the opposite direction to the applied voltage. For this reason, the mutual inductance opposes the self inductance, and the resulting inductance of the coil is reduced. This analysis matches the blocked impedance described above because it assumes passive materials with fixed geometry and magnetic properties. The other value of inductance to consider is when the Galfenol has free-free boundary conditions. This means that there is no force on the Galfenol, so (4.15) can be solved for the difference in velocity of the two ends as,

$$v_2 - v_1 = j\omega c^H \frac{d}{s^H} \left(\frac{2Ni}{\mu^S(\mathcal{R}_s + 2\mathcal{R}_g)} \right). \tag{4.22}$$

This leads to the relationship between the voltage to the coils and the current in the coils as,

$$V = \frac{j\omega N^2 i}{\mathcal{R}_s + 2\mathcal{R}_g} + \frac{dN}{2c^H} \left(j\omega c^H \frac{d}{s^H} \left(\frac{2Ni}{\mu^S(\mathcal{R}_s + 2\mathcal{R}_g)} \right) \right). \tag{4.23}$$

This equation can be simplified by recognizing the relationship to the value of k, coupling term. The simplification shows that,

$$V = j\omega L^S \left(1 + \frac{k^2}{1 - k^2} \right) i. \tag{4.24}$$

The free-free inductance value is thus,

$$L^T = L^S \left(1 + \frac{k^2}{1-k^2}\right). \tag{4.25}$$

The two values of inductance set the limits on the inductance during operation. The blocked inductance represents the lower limit while the free-free inductance shows the upper limit. The difference between the two limits will depend on the material properties of the Galfenol being used.

Now that the inductance of a coil is known, the power in the system can be analyzed. In an AC system, the peak-to-peak power is given as the product of the voltage an current amplitudes. The mean value of power depends on the angle between the voltage and current. The voltage is related to the current through the impedance of the system. For a coil, the main component is the inductance with some resistance, and as mentioned in earlier, some self capacitance. As first analysis of how the magnitude of power can be altered, the self capacitance will be ignored. The resistance will also be ignored because at higher frequencies the inductance term dominates because of the frequency dependence. This leads to the impedance of the coil as,

$$Z = j\omega L. \tag{4.26}$$

Since the two coils are wired in parallel, the actual impedance of the entire system is, $Z = \frac{j\omega L}{2}$. The current in the coils can be solved for a specified value of field in the sample with (4.5). After solving for the current, the current can be shown to be,

$$i = \frac{H(A_g \mu^S (\mathcal{R}_s + 2\mathcal{R}_g)}{2N}. \tag{4.27}$$

Again the total current to the system is affected because the coils are wired in parallel. This means that the current is actually twice the value calculated in (4.27). The peak-to-peak power is given as, $P = i^2|Z|$. This leads to the power being calculated by,

$$\begin{aligned} P &= \left(\frac{HA_g\mu^S(\mathcal{R}_s + 2\mathcal{R}_g)}{N}\right)^2 \left(\frac{1}{2}\frac{N^2}{\mathcal{R}_s + 2\mathcal{R}_g}\left(1 + \frac{k^2}{1-k^2}\right)\right)\omega \\ &= \frac{1}{2}(HA_g\mu^S)^2(\mathcal{R}_s + 2\mathcal{R}_g)\left(1 + \frac{k^2}{1-k^2}\right)\omega \end{aligned} \tag{4.28}$$

This relationship for the power is useful in determining how the transducer should be designed to reduce the magnitude of the power. For a given excitation frequency, the variables that can be adjusted are the cross-sectional area of Gaflenol, the reluctance of the steel, the reluctance of the Galfenol, and the field. The values of k and μ^S are material properties and cannot be adjusted. The current reluctance value of steel is on the order of 10 times smaller than that of the Galfenol, therefore altering the steel reluctance would only slightly affect the power requirements. This is due to the fact that the permeability of the steel is large. The reluctance of Galfenol is given as,

$$\mathcal{R}_g = \frac{l_g}{\mu^S A_g}. \tag{4.29}$$

Since the reluctance of the Galfenol is much larger than the reluctance of steel, changing the length of the Galfenol would lower the power requirements slightly.

Small adjustments to the power could be achieved by using a higher permeability steel such as Mu-metal or Metglass. Decreasing the length of the steel flux return path as well as increasing the area of the path would also help to reduce the power. One potential drawback to decreasing the length and increasing the area would in effect change the geometry of the coil which has been shown to be affect the inductance in single coil applications. The more layers that are present the higher the self

capacitance of the coils and the less reliable they become. The main factor in reducing the power is reducing the current in the system. It should be noted that while these changes reduce the current, they increase the inductance and thus impedance of the system. This could make it necessary for very large voltages. Changing the number of turns does not have a direct impact on the power; however, fewer turns would mean a smaller impedance and voltage with the drawback of increasing the current. The two values should be balanced depending on the power source available. The current will be limited by the type of wire used such that the coils do not overheat and burn out.

From (4.28) it can be seen that the largest change would come from changing the field in the material. Since the field is squared, a small change in the field will result in a larger change in the power. The area is also squared; however, the area appears in the denominator of the reluctance term, and the overall change in the power is more closely related to the area rather than the square of the area. The downside of reducing the field is that this will affect the response of the system. To determine how the change in field would affect the change in power as well as the output response, a modulation test was conducted with different fields for the carrier wave.

The carrier wave was adjusted such that the field amplitude in the sample was approximately 0.25 kA/m, 0.50 kA/m, 0.75 kA/m, and 1 kA/m with a frequency of 5 kHz. A stress signal with a mean stress of 5 Mpa and an amplitude of 2.8 MPa at a frequency of 10 Hz was then superimposed on the carrier wave. The resulting modulated signals can be seen in Figure 4.8. It is noted that the output voltage is reduced with a reduction in the field. The change in the output as the stress is applied is also reduced. To compare the signals the amplitude of the demodulated

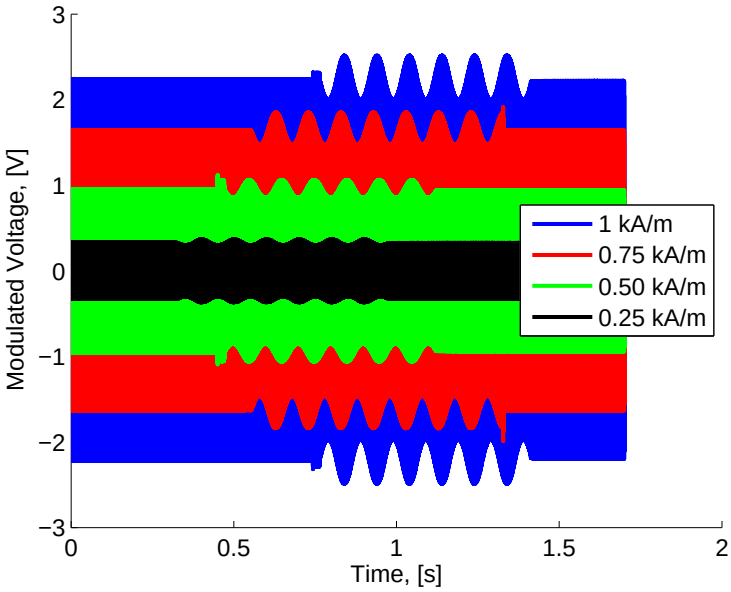

Figure 4.8: Four Different Modulated Signals for Fields of 0.25 kA/m, 0.50 kA/m, 0.75 kA/m, and 1 kA/m

signals was computed. The results of this comparison are shown in Figure 4.9. There is a significant decrease in the voltage amplitude; however there is a sufficient change in the signal with the application of stress, such that the signal could be amplified for use in force sensing applications.

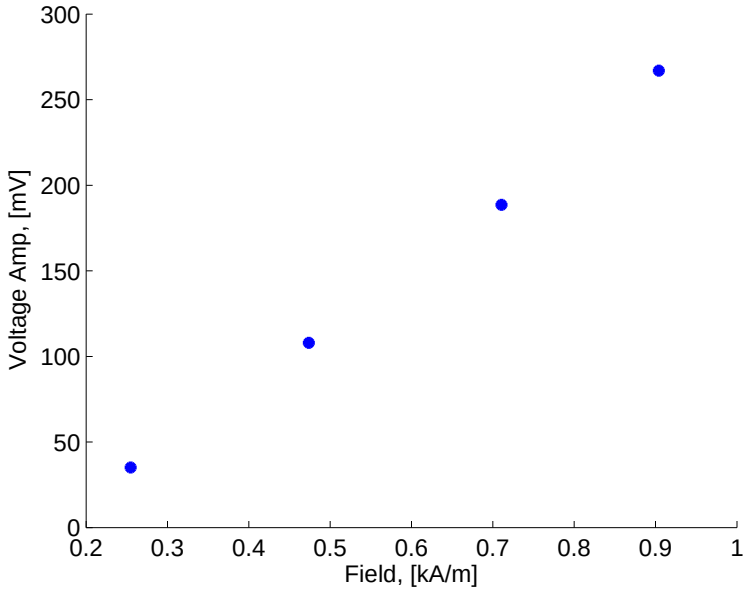

Figure 4.9: Demodulated Voltage Amplitude During Stress Application Versus Carrier Signal Field Amplitude.

The final quantity of interest in this study is the power consumption of the transducer. From (4.28) the relationship between field and power is a quadratic relationship where the power is related to the square of the field strength. Figure 4.10 shows the results of the modulation testing using different fields in the sample. It is clear that the relationship is indeed quadratic and using a field of approximately 0.25 kA/m reduces the peak-to-peak power needed to approximately 0.5 W.

4.5 Summary

This chapter has discussed the electrical power requirements to operate this transducer as a force sensor capable of measuring high frequency forces. This makes use of the modulation technique described in Chapter 3 to create a force sensor that has

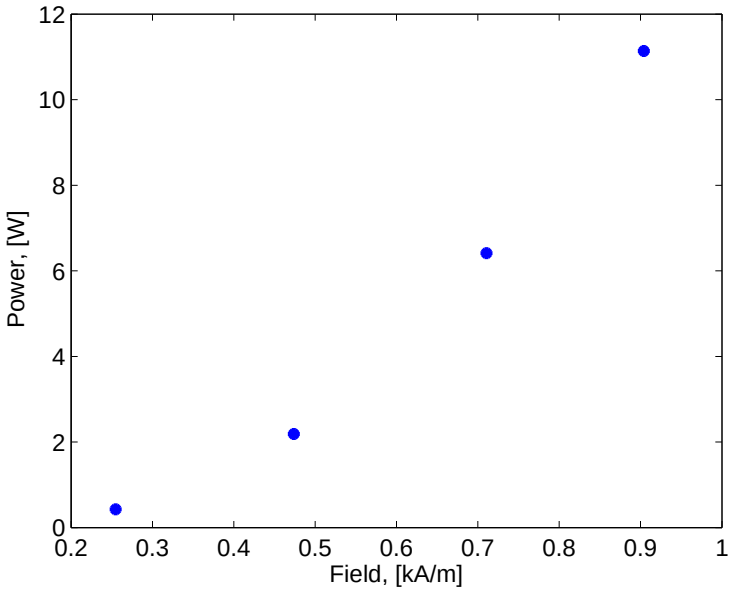

Figure 4.10: Peak-to-peak Power Consumption Versus Carrier Signal Field Amplitude.

an output voltage that is a function of the stress input alone, and not affected by the frequency of the input. The results of the power analysis show that the current transducer requires significant power to generate the carrier wave necessary for sensing. Additional work needs to be completed to optimize the magnetic circuit and excitation coils to reduce the power requirements for a Galfenol based sensor in specific applications. Reducing the power requirements would help the future of these devices by making them more viable solution to current force sensing devices. It is desirable to reduce the power required to operate sensors because they must be in constant operation to measure forces, so ideally the power draw would be small.

Chapter 5: GALFENOL MODELING

5.1 Overview

As mentioned in Chapter 1, the modeling used in this thesis is the Discrete Energy Average Model developed by Evans et al. [14]. This model is based on the laws of thermodynamics, specifically, the free energy of the material. Through careful development and transformation through a Legendre transformation, it can be shown that the free energy is given by,

$$G(\mathbf{H}, \mathbf{T}, \theta) = U(\mathbf{M}, \mathbf{S}, \eta) - \eta\theta - \mathbf{S} \cdot \mathbf{T} - \mu_0 \mathbf{M} \cdot \mathbf{H}. \tag{5.1}$$

The dependencies after the transformation are then

$$\mathbf{M} = \mathbf{M}(\mathbf{H}, \mathbf{T}, \theta, \mathbf{m}^k, \xi^k), \tag{5.2}$$

$$\mathbf{S} = \mathbf{S}(\mathbf{H}, \mathbf{T}, \theta, \mathbf{m}^k, \xi^k), \tag{5.3}$$

$$\eta = \eta(\mathbf{H}, \mathbf{T}, \theta, \mathbf{m}^k, \xi^k). \tag{5.4}$$

where, $\mathbf{T}$ is the stress, $\mathbf{S}$ is the strain (using vector notation), $\mathbf{H}$ is the magnetic field, and $\mathbf{M}$ is the magnetization. Also, θ is the temperature, $\mathbf{m}^k$, possible domain orientations, ξ^k, is the volume fraction of material, η is the entropy, μ_0 is the permeability of free space, and $\mathbf{U}$ is the internal energy.

Using an in depth thermodynamic analysis, the constitutive relationships can be derived. By using the assumptions of an isothermal process, negligible temperature gradients, reversible domain rotation, and irreversible domain volume fraction evolution, it can be shown that the following constitutive relationships determine the system

$$\mu_0 \mathbf{M} = -\frac{\partial G}{\partial \mathbf{H}}, \tag{5.5}$$

$$\mathbf{S} = -\frac{\partial G}{\partial \mathbf{T}}, \tag{5.6}$$

$$\frac{\partial G}{\partial \mathbf{m}^k} = 0, \tag{5.7}$$

$$-\frac{\partial G}{\partial \xi^k}\dot{\xi}^k \geq 0. \tag{5.8}$$

These equations describe the constitutive behavior of the material [14]. Defining the free energy and volume fractions allows for the model to be developed. With the free energy, the magnetization, strain, and possible domain orientations can be calculated. This energy formalization will be described in the following section.

5.2 Discrete Energy Average Method

The first step in the model development was to define the free energy. The free energy is defined locally with three components: magnetic anisotropy G_A, magneto-mechanical coupling G_C, and Zeeman or field energy G_Z. These are expressed by idealizing the complex domain structure as a system of non-interacting, single-domain, Stoner-Wohlfarth (S-W) particles. The local definition depends only on the easy axis, $\mathbf{c}^k$. The free energies are defined as

$$G_A^k = K_0^k + \frac{1}{2}K^k||\mathbf{m}^k - \mathbf{c}^k||^2, \tag{5.9}$$

$$G_C^k = -\lambda^k \cdot \mathbf{H}, \tag{5.10}$$

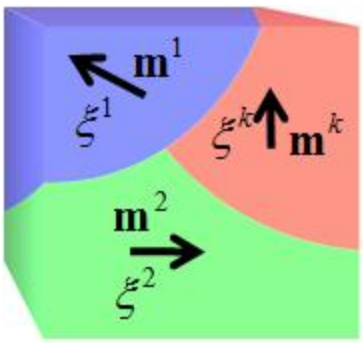

Figure 5.1: Depiction of Domain Orientations and Their Respective Volume Fractions [7]

$$G_Z^k = \mu_0 M_s \mathbf{m}^k \cdot \mathbf{H}. \tag{5.11}$$

The energy is them minimized using a constrained minimization about the easy axis in the material. This leads to the possible domain orientations being defined through,

$$||\mathbf{m}^k|| = 1 \approx \mathbf{c}^k \cdot \mathbf{m}^k = 1. \tag{5.12}$$

For the macroscopic response of the material, the domain orientations are normalized through,

$$\hat{\mathbf{m}}^k = \frac{\mathbf{m}^k}{||\mathbf{m}^k||}. \tag{5.13}$$

With the domain orientations, and free energy known, the volume fractions are the final part needed to solve for magnetization and strain in the sample at the macroscopic level. Figure 5.1 shows a depiction of different domain orientations and their respective volume fractions. The volume fraction is shown to be,

$$\xi^k = \frac{e^{-G^k/\Omega(\xi)}}{\sum_{k=1}^{6} e^{-G^k/\Omega(\xi)}}. \tag{5.14}$$

Equation 5.14 is used with the following equations to find the magnetization and strain of the material. The magnetization is given by,

$$\mathbf{M} = M_s \sum_{k=1}^{6} \xi^k \hat{\mathbf{m}}^k. \tag{5.15}$$

and the strain given by,

$$\mathbf{S} = \sum_{k=1}^{6} \xi^k \mathbf{S}_m^k + s\mathbf{T}. \tag{5.16}$$

This model is an efficient way to determine the response of Galfenol to inputs of magnetic field and stress. The equations described above are implemented into the COMSOL interface through a set of user defined MatLab functions. The functions were developed by Chakrabarti et al. to aid in the design of Galfenol based actuators and sensors [7]. The integration into COMSOL is a powerful tool to testing design ideas.

5.3 Model Parameters

The model parameters include the anisotropy energy; K, the smoothing factor; Ω, saturation magnetostriction in <100> direction; λ_{100}, saturation magnetization; M_s, saturation magnetostriction in <111> direction; λ_{111}, and energy in burst region; K_0. These values can be found by optimizing the model parameters with the experimental data. The experimental data is first used to determine an initial guess of the parameters. Two of the values, M_s and λ_{100}, can be measured directly from experimental data. K is found from the zero field susceptibility through,

$$K = \frac{\mu_0 M_s^2}{\chi(T)} + 3\lambda_{100} T. \tag{5.17}$$

Table 5.1: Discrete Energy Average Model Parameters for 18.4% at. Ga

Parameter	Value	Units
K	27.86	kJ/m^3
Ω	786.19	J/m^3
λ_{100}	157.3	microstrain
$\mu_0 M_s$	1.38	T

and K_0 is found by equating energies of perpendicular and parallel orientations in the burst region through,

$$K_0 = \frac{(\mu_0 M_s H_{burst})^2}{6\lambda_{100}T - 2K} + \frac{3}{2}\lambda_{100}T + \mu_0 M_s H_{burst}. \tag{5.18}$$

Ω cannot be expressed analytically and is bounded from 0.5-30 kJ/m^3. Finally, λ_{111} also cannot be expressed analytically, but does not have an effect on the <100> direction and can therefore be ignored in the optimization process. These properties produce an initial guess for the parameters. The optimization process can then begin using a least squares regression procedure. This process adjusts the different parameters within the bounds of each until the relative error with respect to the range of the data is minimized. Chakrabarti et al. also developed this code in MATLAB to aid in the optimization process [7]. With the experimental data collected as a part of this research for 18.4 % at. Ga, the optimized parameters in Table 5.1 are found.

These values have been used in the subsequent modeling. Figure 5.2 and Figure 5.3 show the model results compared with the experimental results in Chapter 2. The measured field and stress were taken as the inputs to the model, and the magnetization was the output. The model and the data show good agreement. The relative error for the constant current case was 1.62 % and 1.11 % for the constant field.

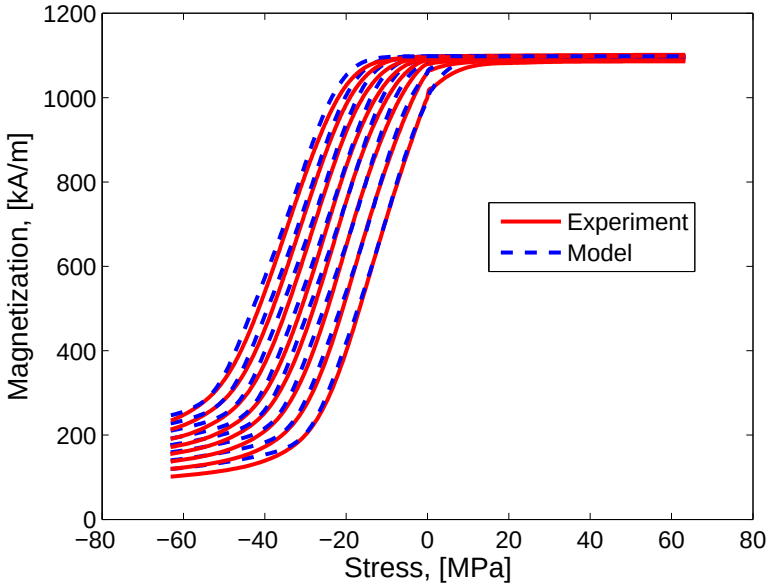

Figure 5.2: Model Comparison with Experimental Results for Constant Current Excitation Using Optimized Model Parameters

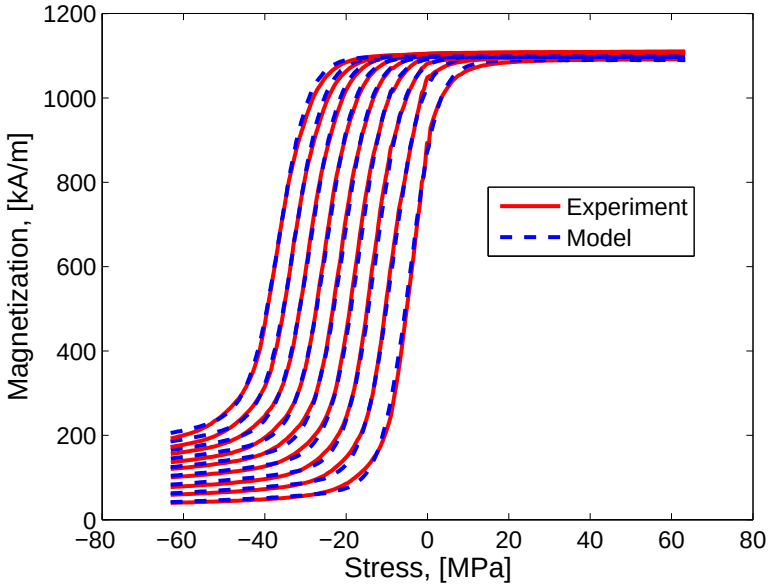

Figure 5.3: Model Comparison with Experimental Results for Constant Field Excitation Using Optimized Model Parameters

5.4 COMSOL Modeling

The model described above was used in conjunction with the COMSOL interface to create a means of modeling the full transducer output. The material model was coded in Matlab and a set of codes was used to implement this model into the COMSOL multi-physics solvers. This allows for the geometry to be created in COMSOL and the appropriate material properties to be selected for each subdomain. Passive materials make use of the linear elastic and linear magnetic equations, while the subdomains of Galfenol take into account the magneto-mechanical coupling as found from the constitutive laws. After applying the appropriate boundary conditions and inputs, the model can be solved and post-processed with the Matlab code to determine the quantities of interest in the Galfenol sample. For the model described above, the input to the system are magnetization **T** and magnetic field **H**. The output of the model is the magnetization **M** and magnetostriction/strain **S**. One can also look at the magnetic flux density **B** instead of magnetization. However, for the COMSOL model, the inputs to the Galfenol subdomain are **B** generated from the excitation coils and **S** from the mechanical action. In order to implement the model into COMSOL, the inverse relationships had to be derived. This inverse relationship was then implemented into COMSOL through the user defined MatLab codes using the Inverse Newton Method [7].

5.4.1 Development

For modeling the transducer in COMSOL, the geometry first had to be created. This was done by creating the steel flux path, galfenol rod, and coils as different subdomains. Figure 5.4 shows a slice of the transducer geometry that was used in

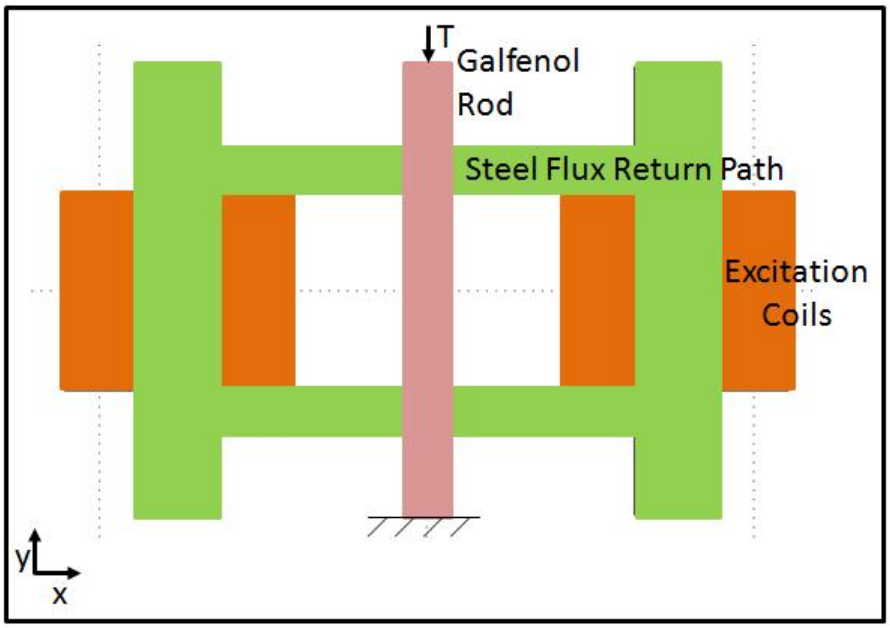

Figure 5.4: COMSOL Geometry of Transducer

the COMSOL model. This figure also shows the boundary conditions used in the model. The stress is applied to the top boundary of the rod while the bottom rod is rigidly fixed. The flux return path and the coils are inactive in the mechanical domain because they are not interacting with the stress at all. The coils were broken into four components for simplifying the assignment of current in each subdomain. Figure 5.5 shows the transducer top view in COMSOL with the current densities labeled. These current densities create a flux in the steel path that then moves into the Galfenol rod at the center. There is also a box of air surrounding the transducer. This box is used to define the vector magnetic potential boundary conditions. On the outside boundaries of the box, the vector magnetic potential ($\mathbf{A}$) is equal to zero.

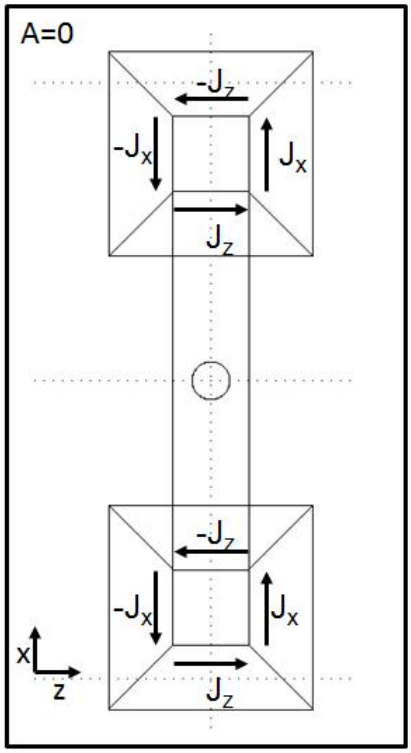

Figure 5.5: COMSOL Definiton of Current Densities

To simulate the major loops, one cycle of a sinusoidal wave was applied so that the stress went from 0 MPa to -65 MPa and back to 0 MPa once again using a cosine function so as to have no discontinuities in the applied stress. This simulation was taken with a total of 80 steps. For the simulation, a constant voltage was applied to the drive coils to create current densities as seen above in Figure 5.5

5.4.2 Results

The COMSOL modeling was performed at various currents and a comparison of several of the currents can be seen below in Figure 5.6. There is good agreement between the model and experiment. This agreement is a good indication that the COMSOL interface can be used in the sensor design process to determine the best geometry for a real-world force sensor. There is some error at lower stresses because of the small change in the flux density at the lower stresses. There is also some variation in the COMSOL results that is caused by the inability of the function to converge. This is again an issue at lower stresses. Further work needs to be done to improve the convergence and thus speed of the modeling functions. There is also some error caused because the small air gaps between the Galfenol and the steel flux return path are ignored.

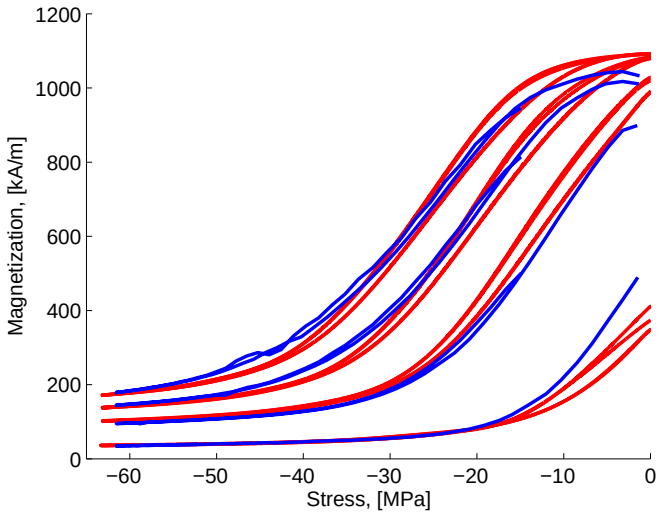

Figure 5.6: Comsol Comparison with Experimental Results for Constant Current Excitation Using Optimized Model Parameters

5.5 Summary

The current COMSOL modeling is still in a preliminary analysis and needs further improvement for speed and accuracy at lower compressive stresses. The agreement between the experimental and simulated data is promising for future applications. COMSOL could be used to aid in the design of a real world sensor. This sensor could integrate a Galfenol component into a structural member to monitor the force in said member. There are several ways to achieve this integration. One possible integration involves creating a cavity in the member into which a Galfenol sample could be placed. Another method would involve creating a groove around the circumference of a cylindrical member and placing a ring of Galfenol in the groove. The use of finite element programs such as COMSOL will be very beneficial to the future of Galfenol applications.

Chapter 6: SUMMARY AND CONCLUSION

6.1 Summary

This thesis has touched on several different aspects involved in the characterization of Galfenol alloys for use in sensing applications. Chapter 2 discussed the quasi-static major loop characterization for the major loops of the material. The magnetic response of the material was monitored and recorded with the application of a mechanical stress input covering a large range of stresses from tension to compression. These curves show the nonlinear and hysteretic behavior of Galfenol. This data was also compared with similar data for minor loop stress input which is more representative of typical applications. The sensitivity of both major and minor loops were compared, and this data was also used to determine the model parameters for this alloy.

Chapter 3 focused on the frequency dependence of Galfenol and how the response varied with the input frequency of the force. The sensitivity decreased with the increase in frequency which is a potential problem for a Galfenol based force sensor. A modulation technique was proposed and tested to show that making use of the stress-dependent susceptibility can aid in the design of force sensors and create a response that is independent of frequency. This modulation technique requires high

frequency excitation of the Galfenol which requires significant power with the current transducer design. Chapter 4 describes the power requirements for the current set up. The impedance of the excitation coils was monitored over a range of frequencies as well as the field strength in the material. This allowed for an estimation of current, voltage, and thus power necessary to generate a specific field strength in the material. This estimation was also compared to the power requirements observed through the high frequency modulation testing conducted in Chapter 3.

It is noted that while care was taken to reduce the error in the data measurements shown in this thesis there are inherent sources or error with any experimental set up. The main source of error is through different instruments used in testing. For the characterization tests, the flux meter, load cell, and hall chip all have different level of accuracy even in perfect situations. These devices were used in ranges such that the accuracy was much smaller than the signal. As an example, the flux meter has an accuracy of approximately 0.005 T while the actual measurements were conducted on the order of 0.1 T. Other potential sources of error are in the test set up. The hall chip measurement assumes the flux is entering the hall chip perpendicularly; however, there is potential for slight misalignment during the installation process. Care was taken to reduce this error by carefully positioning the hall chip and affixing the hall chip to the sample to maintain consistent positioning throughout testing. Other instruments used in the power testing included the voltage monitor on the Techron amplifier and the current clamp. Another source of error in the tests is the Galfenol sample itself. The sample is a <100> orientated sample; however, not every crystal is perfectly aligned with the axis of the rod. There is some variability in orientations

and thus some variability in the material properties of the sample. These will vary from sample to sample and create some differences in measurements.

Chapter 5 takes a look at implementing the characterization data with constitutive models in COMSOL for the design of future Galfenol based devices. The constitutive model employs an energy-averaged method to calculate the response of Galfenol under specific loading conditions. The model is implemented in COMSOL through user defined MATLAB functions to determine the response to a complex system. The geometry is defined, and the material is monitored for the same quantities tested in the actual experiments. This procedure shows good promise for future use in prototype design.

6.2 Future Work

This work focused on the characterization of the alloy under various loading conditions as well as addressing several concerns with a Galfenol based force sensor. Additional work will further help gain an understanding of Galfenol alloys and how they behave in various applications so that they can be implemented into solutions to different problems. The high frequency characterization can be expanded to different bias stress points as well as different fields. The development of a high frequency testing apparatus for major loop testing would also help in the characterization of different alloys and materials. The minor loop testing at high frequencies is helpful; however, it is limited in application due to the limited range of stress used. Another area of potential work would be to look at the modulation technique at high frequencies and the limits on the carrier wave frequency. As was mentioned earlier, this

depends on the type of filter used in the analysis and the desired performance. Further study in the relationship between the carrier wave frequency and the performance would be valuable to future designs.

In addition to the high frequency testing, the power requirements discussed in Chapter 4 of this thesis could be further refined. This chapter shows a significant power requirement for this transducer to operate as a force sensor using the modulation technique. Reducing this power would be instrumental in advancing these materials into practical situations. Further study into the different aspects of the transducer that affect the power is required to gain a better understanding of what can be changed to alter the power requirements. The transducer design can then be optimized to make a Galfenol-based force sensor a viable replacement for the force sensors in use today.

Finally, the COMSOL modeling shows good promise as a means of prototype design; however, further work on the user defined MATLAB functions needs to be done to improve the efficiency and accuracy. The current iteration has issues with low compressive and tensile stresses, as well as convergence at higher fields. These issues lead to longer simulation times which makes the simulations less efficient. Improving the efficiency of the finite element simulations would be beneficial in using this type of a procedure for device design.

Bibliography

[1] W.D. Armstrong. Magnetization and magnetostriction processes in $\mathrm{tb}_{0.27-0.30}\mathrm{dy}_{0.73-0.70}\mathrm{fe}_{1.9-2.0}$. *Journal of Applied Physics*, 81(5), 1997.

[2] J. Atulasimha. *Characterization and Modeling of the Magnetomechanical Behavior of Iron-Gallium Alloys*. PhD thesis, University of Maryland, College Park, MD, 2006.

[3] J. Atulasimha, G. Akhras, and A.B. Flatau. Comprehensive 3d hysteretic magnetomechanical model and its variation with experimental <100> single-crystal iron gallium behavior. *Journal of Applied Physics*, 103, 2003.

[4] J. Atulasimha, A.B. Flatau, and E. Summers. Characterization and energy-based model of the magnetomechanical behavior of polycrystalline iron-gallium alloys. *Smart Materials and Structures*, 16, 2007.

[5] B. Bhattacharya. Terfenol and galfenol: Smart magnetostrictive metals for intelligent transduction. Technical report, Indian Institute of Technology Kanpur, Kanpur, India, 2005.

[6] F. Calkins, A. Flatau, and M. J. Dapino. Overview of magnetostrictive sensor technology. *Journal of Intelligent Material Systems and Structures*, 18, 2007.

[7] S. Chakrabarti. *Modeling of 3D Magnetostrictive Systems with Application to Galfenol and Terfenol-D Transducers*. PhD thesis, The Ohio State University, Columbus, OH, 2011.

[8] L. dalessandro, F. da Silveira Cavalcante, and J. W. Kolar. Self-capacitance of high-voltage transformers. *IEEE: Transactions of Power Electronoics*, 22(5), 2007.

[9] M. J. Dapino. On magnetostrictive materials and their use in adaptive structures. *Structural Engineering and Mechanics*, 17(3):303–329, 2004.

[10] M. J. Dapino, F. Calkins, and A. Faltau. Magnetostrictive devices. In John G. Webster, editor, *Wiley Encyclopedia of Electrical and Electronics Engineering*, pages 278–305. John Wiley & Sons, Inc., New York, NY, 1999.

[11] M. J. Dapino, R. Smith, F. Calkins, and A. Flatau. A magnetoelastic model for villari-effect magnetostrictive sensors. Technical report, Center for Research in Scientific Computation, Raleigh, NC, 2002.

[12] S. Datta, M. Huang, J. Raim, T. Lograsso, and A. Flatau. Effect of thermal history and gallium content on magneto-mechanical properties of iron-gallium alloys. *Materials Science and Engineering*, 435, 2006.

[13] E.O. Doebelin. *Measurement Systems Application and Design*. McGraw Hill Higher Education, 2004.

[14] P. G. Evans. *Nonlinear Magneto-Mechanical Modeling and Characterization of Galfenol and System-Level Modeling of Galfenol-Based Transducers*. PhD thesis, The Ohio State University, Columbus, OH, 2009.

[15] P. G. Evans and M. J. Dapino. State-space constitutive model for magnetization and magnetostiction. *IEE Transactions of Magnetics*, 44(7), 2008.

[16] P. G. Evans and M. J. Dapino. Measurement and modeling of magnetomechanical coupling in magnetostrictive iron-gallium alloys. In *SPIE Proceedings*, volume 7289, 2009.

[17] P. G. Evans and M. J. Dapino. Stress dependent susceptibility of galfenol to force sensing. *Journal of Applied Physcis*, 108(7), 2010.

[18] D. Fleisch. *A Student's Guide to Maxwell's Equations*. Cambridge University Press, 2008.

[19] D. Jiles. *Introduction to Magnetism and Magnetic Materials*. Chapman and Hall, 1995.

[20] R. Kellogg, A. Flatau, A. Clark, M. Won-Fogle, and T. Lograsso. Quasi-static transduction characterization of galfenol. In *2003 ASME International Mechanical Engineering Congress*, 2003.

[21] A. Mahadevan. Force and torque sensing with galfenol alloys. Master's thesis, The Ohio State University, Columbus, OH, 2009.

[22] A. Mahadevan, P. G. Evans, and M. J. Dapino. Stress dependence of magnetic susceptibility on stress in FeGa. *Applied Physics Letters*, 96(1), 2010.

[23] L.W. Matsch. *Capacitors, Magnetic Circuits, and Transformers*. Prentice-Hall, Inc., 1964.

[24] C. Poeppelman. Characterization of magnetostrictive iron-gallium alloys under dynamic conditions. Undergraduate Honors Thesis at The Ohio State University, 2010.

Appendix A: TIME DOMAIN PLOTS OF DYNAMIC CHARACTERIZATION

This appendix shows the time response for the characterization curves. Figure A.1 shows the flux density signal for the major loop response with a constant current excitation and an initial bias field of 4.0 kA/m (50 Oe). Here we can clearly see how the flux density experiences saturation at low compressive and tensile stresses and a small saturation at high compressive stresses. Figure A.2 shows the field response for the same bias field. The field response is more complicated than the flux response with two small bumps at the saturation. There is also a reversal before the field induced saturation. Figure A.3 and Figure A.4 show the flux density and field responses for the constant field excitation cases. Here we can see the more rapid change in the flux density as well as a more pronounced saturation at high compressive stresses. The constant field as achieved by the use of a PI controller. There is some variation around the burst region as the material shifts from saturation to the burst region. Figure A.5 shows the stress input for both the constant current and constant field testing.

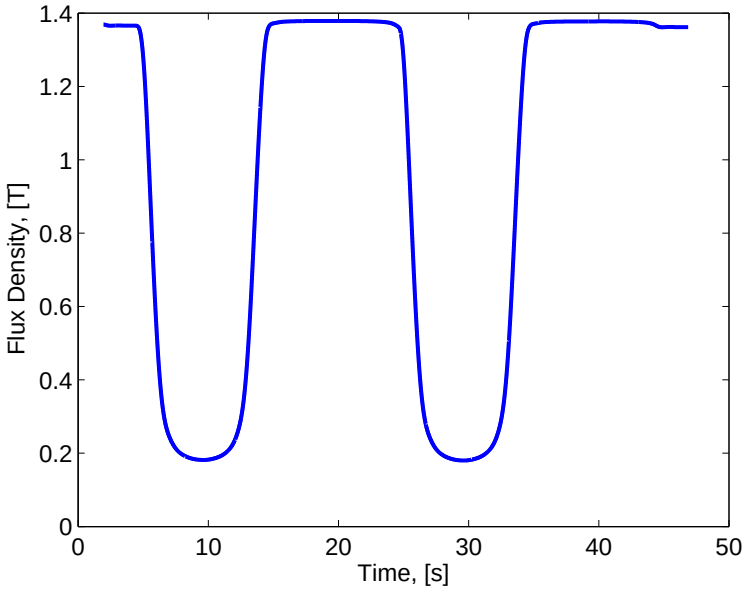

Figure A.1: Major Loop Flux Density Time Signal for Constant Current Excitation with Initial Bias Field of 4.0 kA/m

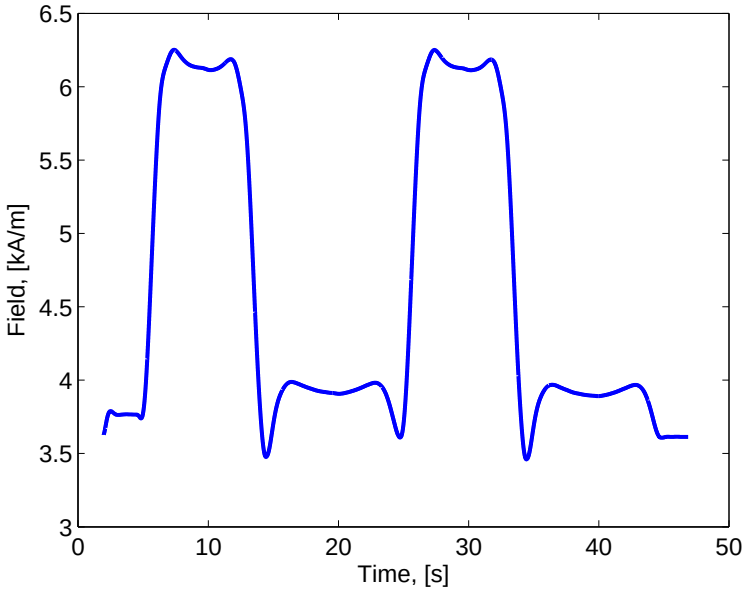

Figure A.2: Major Loop Field Time Signal for Constant Current Excitation with Initial Bias Field of 4.0 kA/m

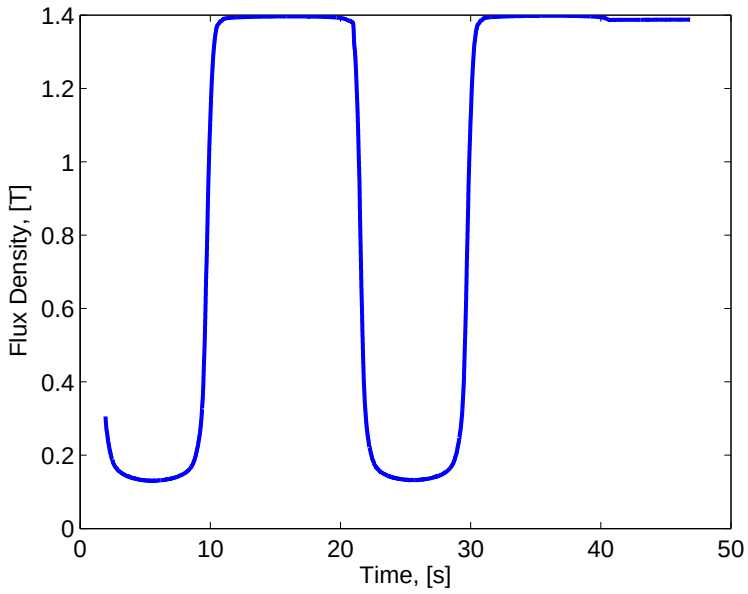

Figure A.3: Major Loop Flux Density Time Signal for Constant Field Excitation with Initial Bias Field of 4.0 kA/m

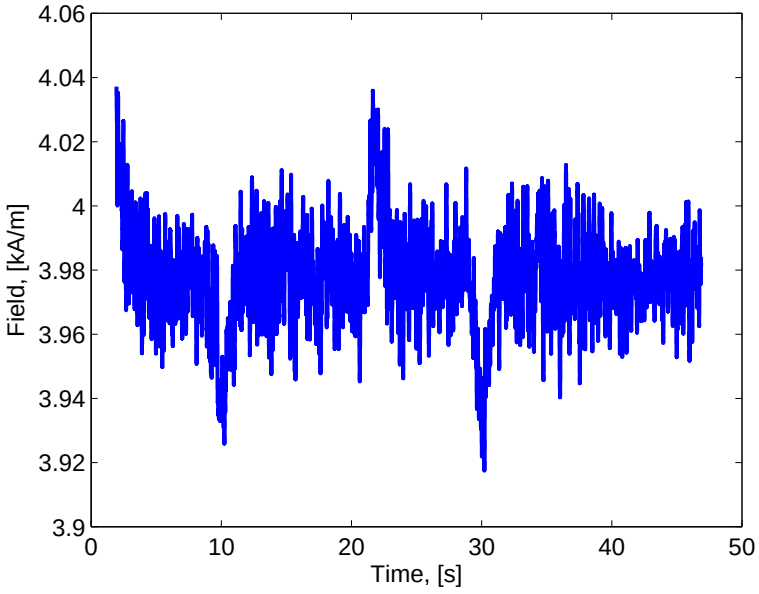

Figure A.4: Major Loop Field Time Signal for Constant Field Excitation with Initial Bias Field of 4.0 kA/m

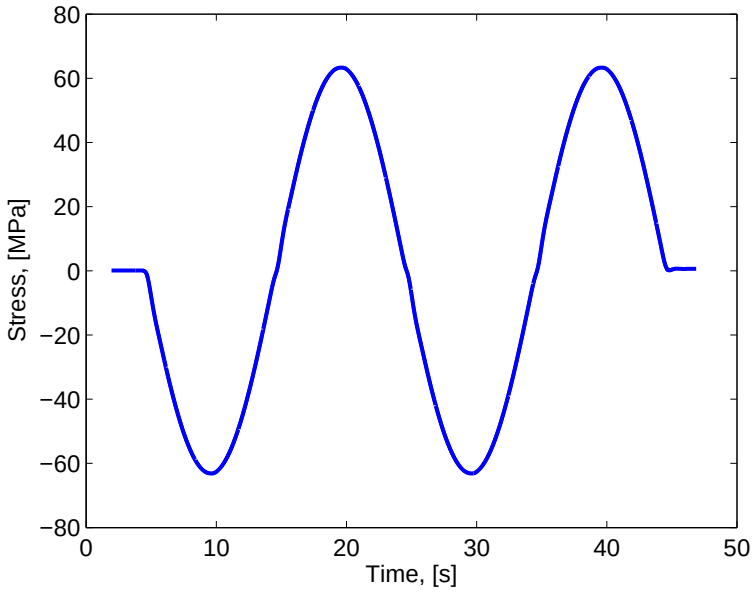

Figure A.5: Major Loop Stress Time Signal for Both Constant Current and Constant Field Testing

For the minor loops, the following figures show similar results for one bias stress point. These figures show the flux density, field, and stress signals for the constant current excitation with an initial bias field of 4.0kA/m (50 Oe) and an initial bias stress of 20 MPa (140 lbf). The constant current tests are shown here to help visualize the minor loop process. Figure A.6 shows the flux density time signal, Figure A.7 shows the field time signal, and Figure A.8 shows the stress time signal for the minor loops.

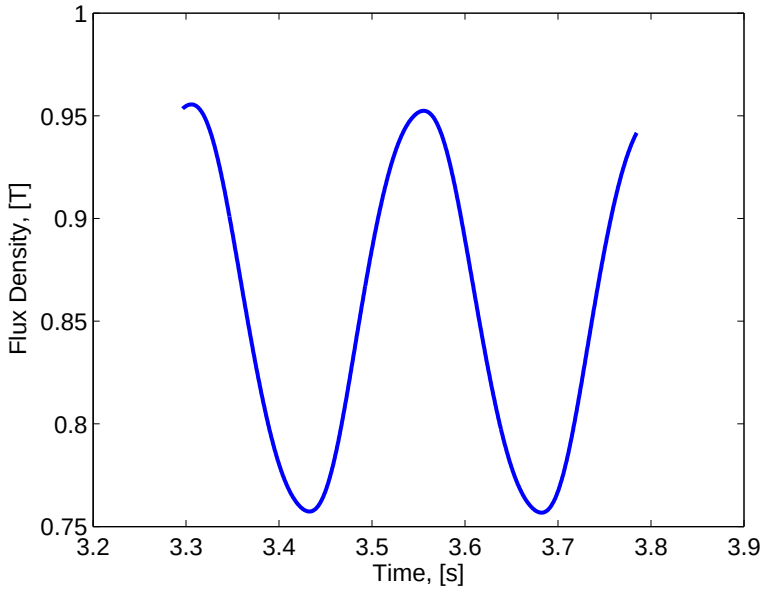

Figure A.6: Minor Loop Flux Density Time Signal for Constant Current Excitation with Initial Bias Field of 4.0 kA/m

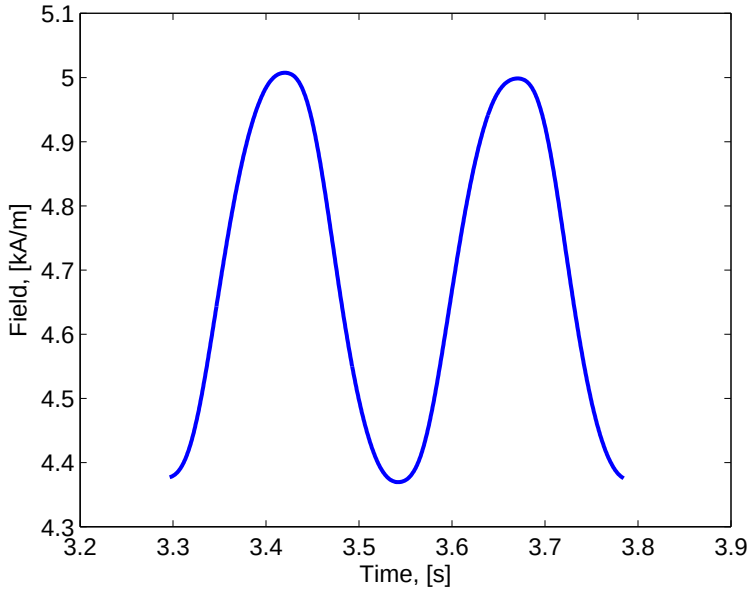

Figure A.7: Minor Loop Field Time Signal for Constant Current Excitation with Initial Bias Field of 4.0 kA/m

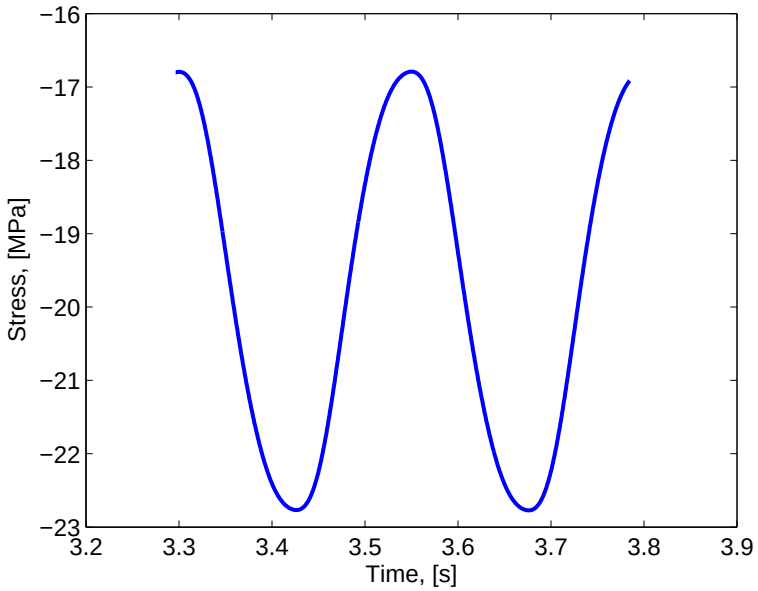

Figure A.8: Minor Loop Stress Time Signal for Both Constant Current and Constant Field Testing

Appendix B: HIGH FREQUENCY TESTING

B.1 High Frequency Characterization

B.1.1 Characterization with Pre-Stress

The results of the characterization using the pre-stress mechanism contain a kink at higher frequencies. As described in Chapter 3, this is due to the tolerances of the device and the interaction of the different components at higher frequencies. Figure B.1 shows the flux density versus stress input with the kinks indicated by the arrows. In looking at the time signals of the data, this kink is caused by a kink in the forcing signal as seen in Figure B.2. In these tests, the bias stress was set to approximately -14 Mpa with an amplitude of approximately 2.2 MPa.

B.1.2 Stepped Sine and Discrete Frequency Comparison

To compare the results obtained with the stepped sine test to those obtained at discrete frequencies, the transfer function was used in conjunction with the forcing signal for the discrete frequency tests. The forcing signals were analyzed for amplitude and mean value. The amplitude was then multiplied by the transfer function to obtain a flux density signal. The mean value for the stress and flux density was calculated

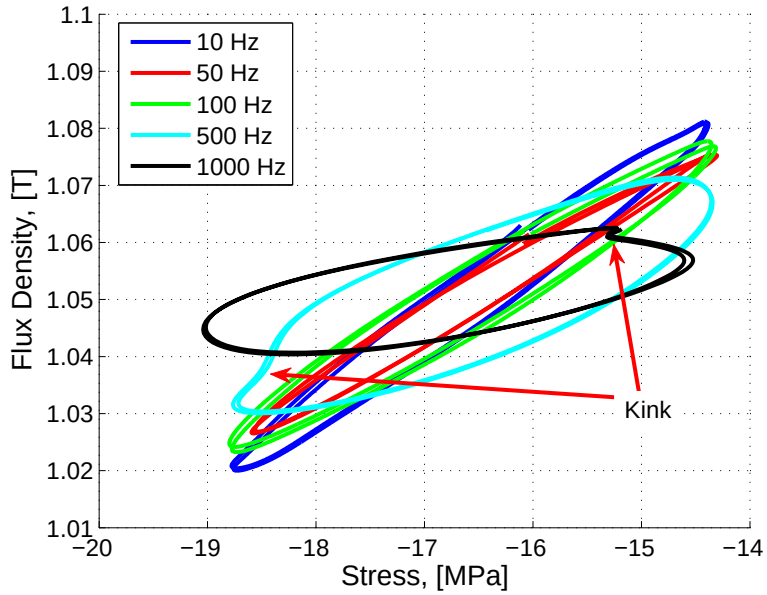

Figure B.1: Flux Density vs Stress with approximately 15 MPa Bias Stress

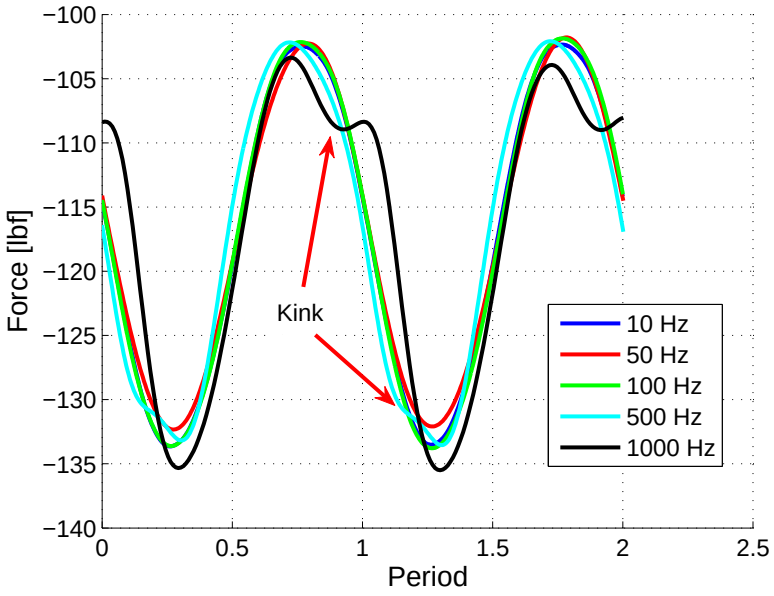

Figure B.2: Forcing Signal Time Response

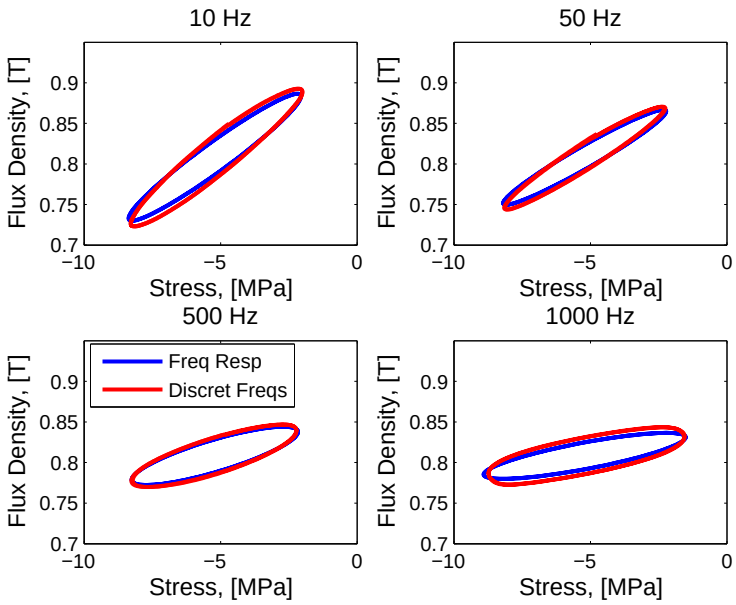

Figure B.3: Flux Density versus Stress for Four Frequencies (10 Hz, 50 Hz, 500 Hz, and 1000 Hz)

from the discrete frequency tests and applied to the results of the multiplication as well. Figure B.3 shows the results of this comparison. This figure shows that both the sensitivity and hysteresis are very similar between the two curves. This provides confidence for the results obtained using the stepped sine test.

B.2 High Frequency Modulation

For the high frequency modulation without controlling the forcing amplitude, there is significant difference in the amplitude and thus the output voltage of the signal. In just looking at the voltage output, the data looks quite noisy; however, when normalizing each voltage with the corresponding of forcing input, the voltage signal is once again flat. Figure B.4 shows the voltage amplitude while Figure B.5

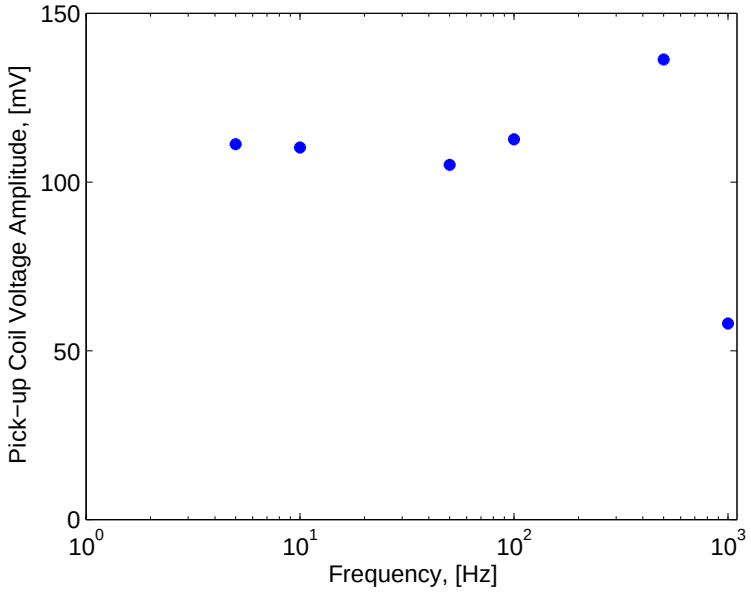

Figure B.4: Voltage Amplitude versus Frequency for Uncontrolled Force Signal

shows the forcing amplitude. It can be seen that there is a similar trend in the of voltage and force. To create an equivalent comparison across the range of frequencies, the voltage was divided by the force and the results shown in Figure B.6. This again shows that the modulation scheme is useful in attempting to use Galfenol in force sensing applications.

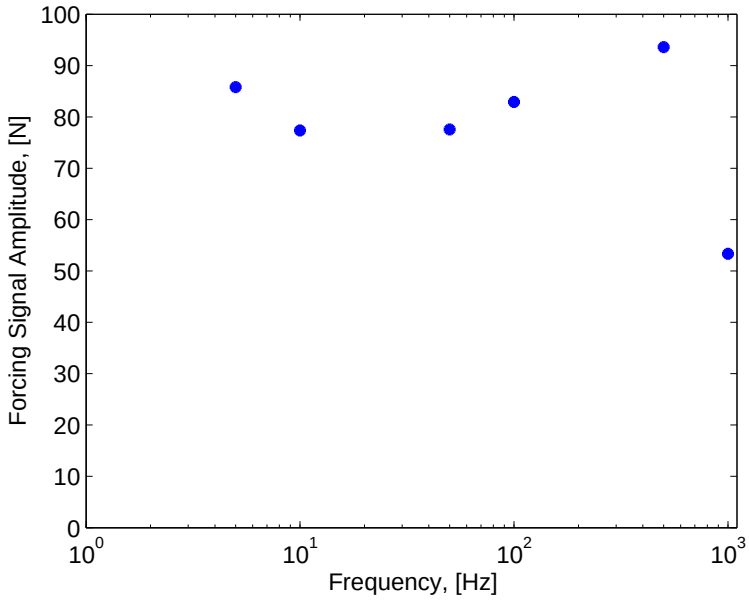

Figure B.5: Force Amplitude versus Frequency for Uncontrolled Force Signal

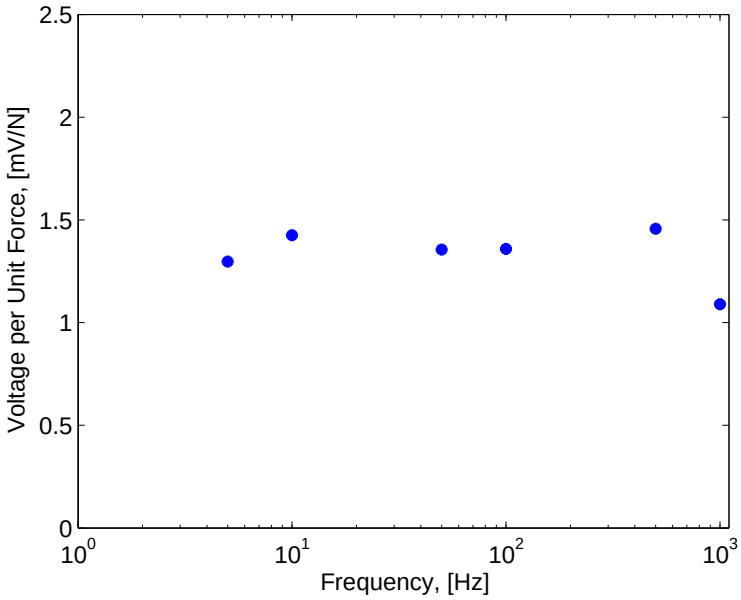

Figure B.6: Voltage per Unit Force versus Frequency for Uncontrolled Force Signal